

1 **H₂SO₄-H₂O-NH₃ ternary ion-mediated nucleation (TIMN): Kinetic-based model and**
2 **comparison with CLOUD measurements**

3
4 Fangqun Yu¹, Alexey B. Nadykto^{1,2}, Jason Herb¹, Gan Luo¹, Kirill M. Nazarenko², and
5 Lyudmila A. Uvarova²

6 Correspondence to: F. Yu (fyu@albany.edu)

7
8 ¹ Atmospheric Sciences Research Center, University at Albany, Albany, New York, US

9 ² Department of Applied Mathematics, Moscow State Univ. of Technology “Stankin”, Russia

10
11
12 **Abstract.** New particle formation (NPF) is known to be an important source of atmospheric
13 particles that impacts air quality, hydrological cycle, and climate. Although laboratory
14 measurements indicate that ammonia enhances NPF, the physico-chemical processes underlying
15 the observed effect of ammonia on NPF are yet to be understood. Here we present a comprehensive
16 kinetically-based H₂SO₄-H₂O-NH₃ ternary ion-mediated nucleation (TIMN) model that is based
17 on the thermodynamic data derived from both quantum-chemical calculations and laboratory
18 measurements. NH₃ was found to reduce nucleation barriers for neutral, positively charged, and
19 negatively charged clusters differently, due to large differences in the binding strength of NH₃,
20 H₂O, and H₂SO₄ to small clusters of different charging states. The model reveals the general favor
21 of nucleation of negative ions, followed by nucleation on positive ions and neutral nucleation, for
22 which higher NH₃ concentrations are needed, in excellent agreement with Cosmics Leaving
23 Outdoor Droplets (CLOUD) measurements. The TIMN model explicitly resolves dependences of
24 nucleation rates on all the key controlling parameters, and captures well the absolute values of
25 nucleation rates as well as the dependence of TIMN rates on concentrations of NH₃ and H₂SO₄,
26 ionization rates, temperature, and relative humidity observed in the well-controlled CLOUD
27 measurements. The kinetic model offers physico-chemical insights into the ternary nucleation
28 process and provides a physics-based approach to calculate TIMN rates under a wide range of
29 atmospheric conditions.

30

31 **1. Introduction**

32 New particle formation (NPF), an important source of particles in the atmosphere, is a dynamic
33 process involving interactions among precursor gas molecules, small clusters, and pre-existing
34 particles (Yu and Turco, 2001; Zhang et al., 2012). H_2SO_4 and H_2O are known to play an important
35 role in atmospheric particle formation (e.g., Doyle, 1961). In typical atmospheric conditions, the
36 species dominating the formation and growth of small clusters is H_2SO_4 . The contribution of H_2O
37 to the nucleation is related to the hydration of H_2SO_4 clusters (or, in the other words, modification
38 of the composition of nucleating clusters) that reduces the H_2SO_4 vapor pressure and hence
39 diminishes the evaporation of H_2SO_4 from the pre-nucleation clusters. NH_3 , the most abundant
40 gas-phase base molecule in the atmosphere and a very efficient neutralizer of sulfuric acid
41 solutions, has long been proposed to enhance nucleation in the lower troposphere (Coffman and
42 Hegg, 1995) although it has been well recognized that earlier versions of classical ternary
43 nucleation model (Coffman and Hegg, 1995; Korhonen et al., 1999; Napari et al., 2002)
44 significantly over-predict the effect of ammonia (Yu, 2006a; Merikanto et al., 2007; Zhang et al.,
45 2010).

46 The impacts of NH_3 on NPF have been investigated in a number of laboratory studies (Kim et
47 al., 1998; Ball et al., 1999; Hanson and Eisele, 2002; Benson et al., 2009; Kirkby et al., 2011;
48 Zollner et al., 2012; Froyd and Lovejoy, 2012; Glasoe et al., 2015; Schobesberger et al., 2015;
49 Kurten et al., 2016) including those recently conducted at the European Organization for Nuclear
50 Research (CERN) in the framework of the CLOUD (Cosmics Leaving Outdoor Droplets)
51 experiment that has provided a unique dataset for quantitatively examining the dependences of
52 ternary H_2SO_4 - H_2O - NH_3 nucleation rates on concentrations of NH_3 ($[\text{NH}_3]$) and H_2SO_4
53 ($[\text{H}_2\text{SO}_4]$), ionization rate (Q), temperature (T), and relative humidity (RH) (Kirkby et al., 2011;
54 Kurten et al., 2016). The experimental conditions in the CLOUD chamber, a 26.1 m³ stainless steel
55 cylinder, were well controlled, while impacts of potential contaminants were minimized
56 (Schnitzhofer et al., 2014; Duplissy et al., 2016). Based on CLOUD measurements in H_2SO_4 - H_2O -
57 NH_3 vapor mixtures, Kirkby et al. (2011) reported that an increase of $[\text{NH}_3]$ from ~0.03 ppb (parts
58 per billion, by volume) to ~0.2 ppb can enhance ion-mediated (or induced) nucleation rate by 2-3
59 orders of magnitude and that the ion-mediated nucleation rate is a factor of 2 to >10 higher than
60 that of neutral nucleation under typical level of contamination by amines. In the presence of
61 ionization, highly polar common atmospheric nucleation precursors such as H_2SO_4 , H_2O , and NH_3
62 molecules tend to cluster around ions; and charged clusters are generally much more stable than
63 their neutral counterparts with enhanced growth rates as a result of dipole-charge interactions (Yu
64 and Turco, 2001).

65 Despite of various laboratory measurements indicating that ammonia enhances NPF, the
66 physico-chemical processes underlying the observed different effects of ammonia on the formation
67 of neutral, positively charged and negatively charged clusters (Schobesberger et al., 2015) are yet
68 to be understood. To achieve such an understanding, a nucleation model based on the first
69 principles is needed. Such a model is also necessary to extrapolate data obtained in a limited
70 number of experimental conditions to a wide range of atmospheric conditions, where $[\text{NH}_3]$,
71 $[\text{H}_2\text{SO}_4]$, ionization rates, T, RH and surface areas of preexisting particles vary widely depending
72 on the region, pollution level and season. The present work aims to address these issues by
73 developing a kinetically-based $\text{H}_2\text{SO}_4\text{-H}_2\text{O-NH}_3$ ternary ion-mediated nucleation (TIMN) model
74 that is based on the molecular clustering thermodynamic data. The model predictions are compared
75 with relevant CLOUD measurements and previous studies.

76

77 **2. Kinetic-based $\text{H}_2\text{SO}_4\text{-H}_2\text{O-NH}_3$ ternary ion-mediated nucleation (TIMN) model**

78 2.1. Background

79 Most nucleation models developed in the past for $\text{H}_2\text{SO}_4\text{-H}_2\text{O}$ binary homogeneous nucleation
80 (e.g., Vehkamäki et al., 2002), $\text{H}_2\text{SO}_4\text{-H}_2\text{O}$ ion-induced nucleation (e.g., Hamill et al., 1982; Raes
81 et al., 1986; Laakso et al., 2003), and $\text{H}_2\text{SO}_4\text{-H}_2\text{O-NH}_3$ ternary homogeneous nucleation (Coffman
82 and Hegg, 1995; Korhonen et al., 1999; Napari et al., 2002) have been based on the classical
83 approach, which employs capillarity approximation (i.e., assuming that small clusters have same
84 properties as bulk) and calculate nucleation rates according to the free energy change associated
85 with the formation of a “critical embryo”. Yu and Turco (1997, 2000, 2001) developed a neutral
86 and charged binary $\text{H}_2\text{SO}_4\text{-H}_2\text{O}$ nucleation model using a kinetic approach that explicitly treats
87 the complex interactions among small air ions, neutral and charged clusters of various sizes,
88 precursor vapor molecules, and pre-existing aerosols. The formation and evolution of cluster size
89 distributions for positively and negatively charged cluster ions and neutral clusters affected by
90 ionization, recombination, neutralization, condensation, evaporation, coagulation, and scavenging,
91 has been named as ion-mediated nucleation (IMN) (Yu and Turco, 2000). The IMN theory
92 significantly differs from classical ion-induced nucleation (IIN) theory (e.g., Hamill et al., 1982;
93 Raes et al., 1986; Laakso et al., 2003) which is based on a simple modification of the free energy
94 for the formation of a “critical embryo” by including the electrostatic potential energy induced by
95 the embedded charge (i.e., Thomson effect (Thomson, 1888)). The classical approach does not
96 properly account for the kinetic limitation to embryo development, enhanced stability and growth
97 of charged clusters associated with dipole-charge interaction (Nadykto and Yu, 2003; Yu, 2005),
98 and the important contribution of neutral clusters resulting from ion-ion recombination to
99 nucleation (Yu and Turco, 2011). In contrast, these important physical processes are explicitly
100 considered in the kinetic-based IMN model (Yu, 2006b).

101 Since the beginning of the century, nucleation models based on kinetic approach have also
102 been developed in a number of research groups (Lovejoy et al., 2004; Sorokin et al., 2006; Chen
103 et al., 2012; Dawson et al., 2012; McGrath et al., 2012). Lovejoy et al. (2004) developed a kinetic
104 ion nucleation model, which explicitly treats the evaporation of small neutral and negatively
105 charged H₂SO₄-H₂O clusters. The thermodynamic data used in their model were obtained from
106 measurements of small ion clusters, ab initio calculations, thermodynamic cycle, and some
107 approximations (adjustment of Gibbs free energy for neutral clusters calculated based on liquid
108 droplet model, interpolation, etc.). Lovejoy et al. (2004) did not consider the nucleation on positive
109 ions. Sorokin et al. (2006) developed an ion-cluster-aerosol kinetic (ICAK) model which uses the
110 thermodynamic data reported in Froyd and Lovejoy (2003a, b) and empirical correction terms
111 proposed by Lovejoy et al. (2004). Sorokin et al. (2006) used the ICAK model to simulate
112 dynamics of neutral and charged H₂SO₄-H₂O cluster formation and compared the modeling results
113 with their laboratory measurements. Chen et al. (2012) developed an approach for modeling new
114 particle formation based on a sequence of acid-base reactions, with sulfuric acid evaporation rates
115 (from clusters) estimated empirically based on measurements of neutral molecular clusters taken
116 in Mexico City and Atlanta. Dawson et al. (2012) presented a semi-empirical kinetics model for
117 nucleation of methanesulfonic acid (MSA), amines, and water that explicitly accounted for the
118 sequence of reactions leading to formation of stable particles. The kinetic models of Chen et al.
119 (2012) and Dawson et al. (2012) consider only neutral clusters.

120 McGrath et al. (2012) developed the Atmospheric Cluster Dynamics Code (ACDC) to model
121 the cluster kinetics by solving the birth–death equations explicitly, with evaporation rate
122 coefficients derived from formation free energies calculated by quantum chemical methods
123 (Almeida et al., 2013; Olenius et al., 2013). The ACDC model applied to the H₂SO₄-
124 dimethylamine (DMA) system considers 0–4 base molecules and 0–4 sulfuric acid molecules
125 (Almeida et al., 2013). Olenius et al. (2013) applied the ACDC model to simulate the steady-state
126 concentrations and kinetics of neutral, and negatively and positively charged clusters containing
127 up to 5 H₂SO₄ and 5 NH₃ molecules. In ACDC, the nucleation rate is calculated as the rate of
128 clusters growing larger than the upper bounds of the simulated system (i.e., clusters containing 4
129 or 5 H₂SO₄ molecules) (Kurten et al., 2016).

130 The kinetic IMN model developed by Yu and Turco (1997, 2001) explicitly simulates the
131 dynamics of neutral, positively charged, and negatively charged clusters, based on a discrete-
132 sectional bin structure that covers the clusters containing 0, 1, 2, ..., 15, ... H₂SO₄ molecules to
133 particles containing thousands of H₂SO₄ (and H₂O) molecules. In the first version of the kinetic
134 IMN model (Yu and Turco, 1997, 2001), due to the lack of thermodynamic data for the small
135 clusters, the compositions of neutral and charged clusters were assumed to be the same and the
136 evaporation of small clusters was accounted for using a simple adjustment to the condensation

137 accommodation coefficients. Yu (2006b) developed a second-generation IMN model which
138 incorporated newer thermodynamic data (Froyd, 2002; Wilhelm et al., 2004) and physical
139 algorithms (Froyd, 2002; Wilhelm et al., 2004) and explicitly treated the evaporation of neutral
140 and charged clusters. Yu (2007) further improved the IMN model by using two independent
141 measurements (Marti et al., 1997; Hanson and Eisele, 2000) to constrain monomer hydration in
142 the H₂SO₄-H₂O system and by incorporating experimentally determined energetics of small
143 neutral H₂SO₄-H₂O clusters that became available then (Hanson and Lovejoy, 2006; Kazil et al.,
144 2007). The first and second generations of the IMN model were developed for the H₂SO₄-H₂O
145 binary system, although the possible effects of ternary species such as the impact of NH₃ on the
146 stability of both neutral and charged pre-nucleation clusters have been pointed out in these
147 previous studies (Yu and Turco, 2001; Yu, 2006b). The present work extends the previous versions
148 of the IMN model in binary H₂SO₄-H₂O system to ternary H₂SO₄-H₂O-NH₃ system, as described
149 below.

150

151 2.2. Model representation of kinetic ternary nucleation processes

152 Figure 1 schematically illustrates the evolution of charged and neutral clusters/droplets
153 explicitly simulated in the kinetic H₂SO₄-H₂O-NH₃ TIMN model. Here, H₂SO₄ (S) is the key
154 atmospheric nucleation precursor driving the TIMN process while ions, H₂O (W), and NH₃ (A)
155 stabilize the H₂SO₄ clusters and enhance in this way H₂SO₄ nucleation rates. Ions also enhance
156 cluster formation rates due to the interaction with polar nucleating species leading to enhanced
157 collision cross sections (Nadykto and Yu, 2003). The airborne ions are generated by galactic
158 cosmic rays (GCRs) or produced by radioactive emanations, lightning, corona discharge,
159 combustion and other ionization sources. The initial negative ions, which are normally assumed to
160 be NO₃⁻, are converted into HSO₄⁻ core ions (i.e., S⁻) and, then, to larger H₂SO₄ clusters in the

161 presence of gaseous H₂SO₄. The initial positive ions H⁺W_w are converted into H⁺A₁₋₂W_w in the
162 presence of NH₃, H⁺S_sW_w in the presence of H₂SO₄, or H⁺A_aS_sW_w in the case, when both NH₃
163 and H₂SO₄ are present in the nucleating vapors. Some of the binary H₂SO₄-H₂O clusters, both
164 neutral and charged, transform into ternary ones by taking up NH₃ vapors. The molar fraction of
165 ternary clusters in nucleating vapors depends on [NH₃], the binding strength of NH₃ to binary and
166 ternary pre-nucleation clusters, cluster composition, and ambient conditions such as T and RH.

167 Similar to the kinetic binary IMN (BIMN) model (Yu, 2006b), the kinetic TIMN model
168 employs a discrete-sectional bin structure to represent clusters/particles. The bin index *i* represent
169 the amount of core component (i.e., H₂SO₄). For small clusters ($i \leq i_d = 30$ in this study), *i* is the

170 number of H₂SO₄ molecules in the cluster (i.e., $i = s$) and the core volume of i^{th} bin $v_i = i \times v_l$, where
 171 v_l is the volume of one H₂SO₄ molecule. When $i > i_d$, $v_i = VRAT_i \times v_{i-1}$, where $VRAT_i$ is the volume
 172 ratio of i^{th} bin to $(i-1)^{\text{th}}$ bin. The discrete-sectional bin structure enables the model to cover a wide
 173 range of sizes of nucleating clusters/particles with the highest possible size resolution for small
 174 clusters (Yu, 2006b). For clusters with a given bin i , the associated amounts of water and NH₃ and
 175 thus the effective radius of each ternary cluster are calculated based on the equilibrium of
 176 clusters/particles with the water vapor and/or ammonia, as described in later sections.

177 The evolution of positive, negative, and neutral clusters due to the simultaneous condensation,
 178 evaporation, recombination, coagulation, and other loss processes, is described by the following
 179 differential equations obtained by the modification of those describing for the evolution of binary
 180 H₂SO₄-H₂O system (Yu, 2006b):

$$181 \quad \frac{\partial N_0^+}{\partial t} = Q + \gamma_1^+ N_1^+ - N_0^+ \left(\sum_{j=1}^{i_{\max}} \beta_{i,j}^+ N_j^0 + \sum_{j=0}^{i_{\max}} \eta_{i,j}^+ N_j^+ + \sum_{j=0}^{i_{\max}} \alpha_{0,j}^{+,-} N_j^- \right) - N_0^+ L_0^+ \quad (1)$$

$$182 \quad \frac{\partial N_0^-}{\partial t} = Q + \gamma_1^- N_1^- - N_0^- \left(\sum_{j=1}^{i_{\max}} \beta_{i,j}^- N_j^0 + \sum_{j=0}^{i_{\max}} \eta_{i,j}^- N_j^- + \sum_{j=0}^{i_{\max}} \alpha_{0,j}^{-,+} N_j^+ \right) - N_0^- L_0^- \quad (2)$$

$$183 \quad \frac{\partial N_1^0}{\partial t} = P_{\text{H}_2\text{SO}_4} + \sum_{j=2}^{i_{\max}} \delta_{j,2} \gamma_j^0 N_j^0 + \sum_{j=1}^{i_{\max}} (\gamma_j^+ N_j^+ + \gamma_j^- N_j^-) - N_1^0 \left(\sum_{j=1}^{i_{\max}} (1 - f_{1,j,1}) \beta_{1,j}^0 N_j^0 + \sum_{j=0}^{i_{\max}} (\beta_{j,1}^+ N_j^+ + \beta_{j,1}^- N_j^-) \right) - N_1^0 L_1^0 \quad (3)$$

$$184 \quad \frac{\partial N_i^+(i \geq 1)}{\partial t} = g_{i+1,i} \gamma_{i+1}^+ N_{i+1}^+ - g_{i,i-1} \gamma_i^+ N_i^+ + \sum_{j=0}^{i-1} \sum_{k=1}^i \frac{v_j}{v_i} f_{j,k,i} \beta_{j,k}^+ N_j^+ N_k^0 + \sum_{j=0}^{i-1} \sum_{k=0}^i \frac{v_j}{v_i} f_{j,k,i} \eta_{j,k}^+ N_j^+ N_k^+ + \sum_{j=0}^i \sum_{k=1}^i \frac{v_k}{v_i} f_{j,k,i} \beta_{j,k}^+ N_j^+ N_k^0 - N_i^+ \left(\sum_{j=1}^{i_{\max}} (1 - f_{i,j,i}) \beta_{i,j}^+ N_j^0 + \sum_{j=0}^{i_{\max}} (1 - f_{i,j,i}) \eta_{i,j}^+ N_j^+ + \sum_{j=0}^{i_{\max}} \alpha_{i,j}^{+,-} N_j^- \right) - N_i^+ L_i^+ \quad (4)$$

$$185 \quad \frac{\partial N_i^-(i \geq 1)}{\partial t} = g_{i+1,i} \gamma_{i+1}^- N_{i+1}^- - g_{i,i-1} \gamma_i^- N_i^- + \sum_{j=0}^{i-1} \sum_{k=1}^i \frac{v_j}{v_i} f_{j,k,i} \beta_{j,k}^- N_j^- N_k^0 + \sum_{j=0}^{i-1} \sum_{k=0}^i \frac{v_j}{v_i} f_{j,k,i} \eta_{j,k}^- N_j^- N_k^- + \sum_{j=0}^i \sum_{k=1}^i \frac{v_k}{v_i} f_{j,k,i} \beta_{j,k}^- N_j^- N_k^0 - N_i^- \left(\sum_{j=1}^{i_{\max}} (1 - f_{i,j,i}) \beta_{i,j}^- N_j^0 + \sum_{j=0}^{i_{\max}} (1 - f_{i,j,i}) \eta_{i,j}^- N_j^- + \sum_{j=0}^{i_{\max}} \alpha_{i,j}^{-,+} N_j^+ \right) - N_i^- L_i^- \quad (5)$$

$$186 \quad \frac{\partial N_i^0(i \geq 2)}{\partial t} = g_{i+1,i} \gamma_{i+1}^0 N_{i+1}^0 - g_{i,i-1} \gamma_i^0 N_i^0 + \sum_{j=lk=1}^{i-1} \sum_{k=1}^{i-1} \frac{v_k}{v_i} f_{j,k,i} \beta_{j,k}^0 N_j^0 N_k^0 + \sum_{j=0}^i \sum_{k=0}^i f_{j,k,i} \alpha_{j,k}^{+,-} \left(\frac{v_k}{v_i} N_j^+ N_k^- + \frac{v_j}{v_i} N_j^- N_k^+ \right) - N_i^0 \left(\sum_{j=1}^{i_{\max}} (1 - f_{i,j,i}) \beta_{i,j}^0 N_j^0 + \sum_{j=0}^{i_{\max}} (\beta_{j,i}^+ N_j^+ + \beta_{j,i}^- N_j^-) \right) - N_i^0 L_i^0 \quad (6)$$

187

188 In Eqs. (1-6), the superscripts “+”, “-”, and “0” refer to positive, negative, and neutral clusters,
 189 respectively, while subscripts i, j, k represent the bin indexes. $N_0^{+,-}$ and Q are the concentration of
 190 initial ions not containing H_2SO_4 (i.e., $\text{H}^+\text{A}_a\text{W}_w$ and NO_3^-) and the ionization rate, respectively. N_i
 191 is the total number concentration (cm^{-3}) of all cluster/particles (binary + ternary) in the bin i . For
 192 small clusters ($i \leq i_d$), N_i is the number concentration (cm^{-3}) of all clusters containing i H_2SO_4
 193 molecules. For example, N_1^0 is the total concentration of binary and ternary neutral clusters
 194 containing one H_2SO_4 molecules. Index i in Eq. (5) refers to the sum of H_2SO_4 and HSO_4^- . The
 195 second term of Eq. (2) describes the reaction of $\text{HSO}_4^- + \text{HNO}_3 \rightarrow \text{NO}_3^- + \text{H}_2\text{SO}_4$. Although the
 196 rate of this reaction is generally negligible, we keep the term there for completeness. $P_{\text{H}_2\text{SO}_4}$ is the
 197 gas-phase production rate of neutral H_2SO_4 molecules. $L_i^{+,-,0}$ is the loss rate due to scavenging by
 198 pre-existing particles, and wall and dilution losses in the laboratory chamber studies (Kirkby et al.,
 199 2011; Olenius et al., 2013; Kurten et al., 2016). $f_{j,k,i}$ is the volume fraction of intermediate particles
 200 (volume = $v_j + v_k$) partitioned into bin i with respect to the core component – H_2SO_4 , as defined in
 201 Jacobson et al. (1994). $g_{i+1,i} = v_1 / (v_{i+1} - v_i)$ is the volume fraction of intermediate particles of
 202 volume ($v_{i+1} - v_i$) partitioned into bin i . $\delta_{j,2} = 2$ at $j=2$ and $\delta_{j,2} = 1$ at $j \neq 2$. $\gamma_i^+, \gamma_i^-,$ and γ_i^0 are the
 203 mean (or effective) cluster evaporation coefficients for positive, negative and neutral clusters in
 204 bin i , respectively. $\beta_{i,j}^+, \beta_{i,j}^-, \beta_{i,j}^0$ are the coagulation kernels for the neutral clusters/particles in
 205 bin j interacting with positive, negative, and neutral clusters/particles in bin i , respectively, which
 206 reduce to the condensation coefficients for H_2SO_4 monomers at $j=1$. $\eta_{j,k}^+$ and $\eta_{j,k}^-$ are
 207 coagulation kernels for clusters/particles of like sign from bin j and clusters/particles from bin k .
 208 It should be noted that the electrostatic repulsion is too strong for small clusters to gain more than
 209 one charge. However, small charged clusters can be scavenged by large pre-existing particles of
 210 same polarity. Large pre-existing particles serve as the sink for small clusters in the model and the
 211 effect of multiple charge is small and thus is not tracked. $\alpha_{i,j}^{+,-}$ is the recombination coefficient
 212 for positive clusters/particles in bin i interacting with negative clusters/particles in bin j , while
 213 $\alpha_{i,j}^{-,+}$ is the recombination coefficient negative clusters/particles from bin i interacting with
 214 positively charged clusters/particles from bin j .

215 The methods for calculating β , γ , η , and α for binary H₂SO₄-H₂O clusters have been described
 216 in our previous publications (Yu and Turco, 2001; Nadykto and Yu, 2003; Yu, 2006b). Dipole-
 217 charge interaction (Nadykto and Yu, 2003), image capture and three-body trapping effects (Hoppel
 218 and Frick, 1986) are considered in the calculation of these coefficients. Since β , η , and α depend
 219 on the cluster mass (or size) rather than on the cluster composition, schemes for calculating these
 220 properties in binary and ternary clusters are identical. In contrast, γ is quite sensitive to cluster
 221 composition. The evaporation rate coefficient of H₂SO₄ molecules from clusters containing i
 222 H₂SO₄ molecules (γ_i) is largely controlled by the stepwise Gibbs free energy change $\Delta G_{i-1,i}$ of
 223 formation of an i -mer from an $(i-1)$ -mer (Yu, 2007)

$$224 \quad \gamma_i = \beta_{i-1} N^0 \exp\left(\frac{\Delta G_{i-1,i}}{RT}\right) \quad (7)$$

$$225 \quad \Delta G_{k-1,k} = \Delta H_{k-1,k}^0 - T\Delta S_{k-1,k}^0 \quad (8)$$

226 where R is the molar gas constant, N^0 is the arbitrary number concentration of a hypothetical gas
 227 consisting solely of the species for which the calculation is performed (generally under the
 228 reference vapor pressure P of 1 atm). ΔH^0 and ΔS^0 are enthalpy and entropy changes under the
 229 standard conditions ($T=298$ K, $P=1$ atm), respectively. The temperature dependence of ΔH^0 and
 230 ΔS^0 , which is generally small and typically negligible over the temperature range of interest
 231 (Nadykto et al., 2009), was not considered.

232

233 2.3. Thermochemical data of neutral and charged binary and ternary clusters

234 ΔH , ΔS and ΔG values needed to calculate cluster evaporation rates (Eq. 7) for the TIMN
 235 model can be derived from laboratory measurements and computational quantum chemistry (QC)
 236 calculation. Thermochemical properties of neutral and charged binary and ternary clusters
 237 obtained using the computational chemical methods and comparisons of computed energies with
 238 available experimental data and semi-experimental estimates are given in Tables A1-A4 and
 239 discussed in Appendix. As an example, Figure 2 shows ΔG associated with the addition of water
 240 (ΔG_{+W}^0), ammonia (ΔG_{+A}^0), and sulfuric acid (ΔG_{+S}^0) to binary and ternary clusters as a function of
 241 the cluster hydration number w . H₂O has high proton affinity and, thus, H₂O is strongly bonded to
 242 all positive ions with low w . ΔG_{+W}^0 expectedly becomes less negative and binding of H₂O to binary
 243 and ternary clusters weakens due to the screening effect as the hydration number w is growing

244 (Fig. 2a). The presence of NH₃ in the clusters weakens binding of H₂O to positive ions. For
245 example, ΔG_{+W}^0 for H⁺A₁W_wS₁ is ~3-4 kcal mol⁻¹ less negative than that for H⁺W_wS₁ at $w=3-6$.
246 The addition of one more NH₃ to the clusters to form H⁺A₂W_w and H⁺A₂W_wS₁ further weakens
247 H₂O binding by ~1.5-6 kcal mol⁻¹ at $w=1-3$, while exhibiting much smaller impact on hydration
248 free energies at $w>3$. Both the absolute values and trends in ΔG_{+W}^0 derived from calculations are
249 in agreement with the laboratory measurements within the uncertainty range of ~1-2 kcal mol⁻¹ for
250 both QC calculations and measurements. This confirms the efficiency and precision of QC
251 methods in calculating thermodynamic data needed for the development of nucleation models.

252 The proton affinity of NH₃ is 204.1 kcal mol⁻¹, which is 37.5 kcal mol⁻¹ higher than that of
253 H₂O (166.6 kcal mol⁻¹) (Jolly, 1991). The hydrated hydronium ions (H⁺W_w) are easily converted
254 to H⁺A₁W_w in the presence of NH₃. The binding of NH₃ and H₂O molecule to H⁺W_w exhibits a
255 similar pattern. In particular, binding of NH₃ to H⁺W_w decreases as w is growing, with ΔG_{+A}^0 for
256 H⁺A₁W_w ranging from -52.08 kcal mol⁻¹ at $w=1$ to -8.32 kcal mol⁻¹ at $w=9$. The binding of NH₃
257 to H⁺W_wS₁ ions is also quite strong, with ΔG_{+A}^0 for H⁺A₁W_wS₁ ranging from -33.14 kcal mol⁻¹ at
258 $w=1$ and to -10.57 kcal mol⁻¹ at $w=6$. The addition of the NH₃ molecule to H⁺A₁W_w (to form
259 H⁺A₂W_w) is much less favorable thermodynamically than that to H⁺W_w, with the corresponding
260 ΔG_{+A}^0 being -22 kcal mol⁻¹ and -6 kcal mol⁻¹ at $w=2$ and $w=6$, respectively. The ΔG_{+A}^0 values for
261 H⁺A₂W_w are 3-5 kcal mol⁻¹ more negative than the experimental values at $w=0-1$; however, they
262 are pretty close to experimental data at $w=2-3$ (Fig. 2b and Table A2). While it is possible that the
263 QC method overestimates the charge effect on the formation free energies of smallest clusters, the
264 possible overestimation at $w=0-1$ will not affect nucleation calculations because most of H⁺A₂W_w
265 in the atmosphere contain more than 2 water molecules (i.e., $w>2$) due to the strong hydration (see
266 Table A2 and Fig. 2a).

267 A comparison of QC and semi-experimental estimates of ΔG_{+S}^0 values associated with the
268 attachment of H₂SO₄ to positive ions shown in Fig. 2c indicates that computed ΔG_{+S}^0 values agree
269 well with observations for H⁺W_wS₁ and H⁺A₁W_wS₁ but differ by ~2-4 kcal mol⁻¹ from semi-
270 experimental values for H⁺A₂W_wS₁. As seen from Figs. 2a and 2c, the attachment of NH₃ to
271 H⁺W_wS₁ weakens the binding of both H₂O and H₂SO₄ to the clusters. This suggests that the
272 attachment of NH₃ leads to the evaporation of H₂SO₄ and H₂O molecules from the clusters. In
273 other words, H₂SO₄ is less stable in H⁺A₁W_wS₁ than in H⁺W_wS₁ (Fig. 2c). While this may be taken
274 for the indication that NH₃ inhibits nucleation on positive ions at the first look, further calculations
275 show that binding of NH₃ to H⁺A₁W_wS₁ is quite strong (Fig. 2b) and that H₂SO₄ in H⁺A₂W_wS₁
276 cluster is much more stable than that in H⁺A₁W_wS₁, with ΔG_{+S}^0 being by ~7 kcal mol⁻¹ more
277 negative at $w>2$. The H⁺A₂W_wS₁ cluster can also be formed via the attachment of H₂SO₄ to
278 H⁺A₂W_w. In the presence of sufficient concentrations of NH₃, a large fraction of positively charged
279 H₂SO₄ monomers exist in the form of H⁺A₂W_wS₁ and, hence, NH₃ enhances nucleation of positive

280 ions. Since positively charged H_2SO_4 dimers are expected to contain large number of water
281 molecules, we have not yet computed and derived quantum chemical data for these clusters. The
282 CLOUD measurements do indicate that once $\text{H}^+\text{A}_2\text{W}_w\text{S}_1$ are formed, they can continue to grow
283 to larger $\text{H}^+\text{A}_a\text{W}_w\text{S}_s$ clusters along $a=s+1$ pathway (Schobesberger et al., 2015).

284 Figure 2 shows clearly that the calculated values in most cases agree with measurements within
285 the uncertainty range that justifies the application of QC values in the case, when no reliable
286 experimental data are available.

287

288 2.4. Nucleation barriers for neutral/charged clusters and size-dependent evaporation rates

289 Nucleation barriers and cluster evaporation rates are critically important for calculations of
290 nucleation rates. This section describes the methods employed to calculate the evaporation rates
291 of nucleating clusters of variable sizes and compositions (i.e., γ in Eqs. 1-6) in the TIMN model.

292

293 2.4.1 Equilibrium distributions of small binary and ternary clusters

294 In the atmosphere, $[\text{H}_2\text{O}]$ is much higher than $[\text{H}_2\text{SO}_4]$ and, thus, H_2SO_4 clusters/particles are
295 always in equilibrium with water vapor (Yu, 2007). In the lower troposphere, where most of the
296 nucleation events were observed, $[\text{H}_2\text{SO}_4]$ is typically at sub-ppt to ppt level, while $[\text{NH}_3]$ is in the
297 range of sub-ppb to ppb levels (Butler et al., 2016; Warner et al., 2016) (note that, in what follows,
298 all references to vapor mixing ratios – parts per billion and parts per trillion – are by volume). This
299 means that small ternary clusters can be considered to be in equilibrium with H_2O and NH_3 vapors.
300 Like the previous BIMN model derived assuming equilibrium of binary clusters with water vapor,
301 the present TIMN model treats small clusters containing a given number of H_2SO_4 molecules as
302 being in equilibrium with both H_2O and NH_3 . Their relative concentrations are calculated using
303 the thermodynamic data shown in Tables A1-A4. It should be noted that the system may deviate
304 from equilibrium and the model scheme is probably not suitable when $[\text{NH}_3]$ is less than or close
305 to $[\text{H}_2\text{SO}_4]$. Under such cases, the equilibrium assumption may overestimate nucleation rates.

306 Figure 3 shows the relative abundance (or molar fractions) of small positive, negative, and
307 neutral clusters ($f_{s,a,w}^{+,-,0}$) containing a given number of H_2SO_4 molecules at the ambient temperature
308 of 292 K and three different combinations of RH and $[\text{NH}_3]$ values. As a result of relative
309 instability of H_2SO_4 in $\text{H}^+\text{A}_1\text{W}_w\text{S}_1$ compared to $\text{H}^+\text{W}_w\text{S}_1$ or $\text{H}^+\text{A}_2\text{W}_w\text{S}_1$ (Fig. 2c), most of positive
310 ions with one H_2SO_4 molecule exist in the form of either as $\text{H}^+\text{W}_w\text{S}_1$ or $\text{H}^+\text{A}_2\text{W}_w\text{S}_1$ (i.e, containing
311 either zero or two NH_3 molecules, Fig. 3a). When $[\text{NH}_3]=0.3$ ppb (with $T=292$ K), most of the
312 positive ions containing one H_2SO_4 molecule do not contain NH_3 and their composition is
313 dominated by $\text{H}^+\text{W}_w\text{S}_1$ ($\bar{w}=\sim 7$). At the given T and $[\text{NH}_3]=0.3$ ppb, around 17% of positive ions
314 with one H_2SO_4 molecule contain two NH_3 molecules at RH=38%. The fraction of positive ions
315 containing one H_2SO_4 and two NH_3 molecules decreases to 0.9%, when RH = 90%. At $T=292$ K

316 and RH=38%, the increase in [NH₃] by a factor of 10 to 3 ppb leads to the domination of
317 H⁺A₂W_wS₁ (~95%) in the composition of positively charged H₂SO₄ monomers. As expected, the
318 composition of positive ions and their contribution to nucleation depends on T, RH, and [NH₃].
319 The incorporation of the quantum chemical and experimental clustering thermodynamics in the
320 framework of the kinetic nucleation model enables us to study all these dependencies.

321 As a result of very weak binding of H₂O and NH₃ to small negative ions (Table A4), nearly all
322 negatively charged clusters with $s=0-1$ do not contain water and ammonia (not shown). In the case,
323 when s is growing to 2, all S⁻S₂A_aW_w clusters still do not contain NH₃ (i.e., $a=0$), while only 20-
324 40% of them contain one water molecule ($w=1$) (Fig. 3b). As s further increases to 3, NH₃ begins
325 to get into some of the negatively charged ions. The fraction of S⁻S₃A_aW_w clusters containing one
326 NH₃ molecule is 9% at RH=38% and [NH₃]=0.3ppb, 3% at RH=90% and [NH₃]=0.3 ppb, and
327 50% at RH=38% and [NH₃]=3 ppb. Most of S⁻S₃W_w clusters are hydrated while the fraction of S⁻
328 S₃A_aW_w clusters containing two NH₃ molecules at these ambient conditions is negligible. The
329 fraction of negative cluster ions containing two NH₃ molecules becomes significant at $s=4$ (Fig.
330 3b) and increases from 28% at [NH₃]=0.3 ppb to 80% at [NH₃]=3 ppb at RH=38%. At [NH₃]=0.3
331 ppb, the increase in RH from 38% to 90% reduces the fraction of NH₃ containing S⁻S₃A_aW_w
332 clusters (i.e., $a \geq 1$) from 95% to 70%, demonstrating a significant impact of RH on cluster
333 compositions and emphasizing the importance of accounting for the RH in calculations of ternary
334 nucleation rates.

335 The equilibrium distributions of neutral clusters are presented in Fig. 3c (H₂SO₄ monomers
336 and dimers) and Fig. 3d (H₂SO₄ trimers and tetramers). Hydration is accounted for in the case of
337 monomers and dimers and not included, due to lack of thermodynamic data, in calculations for
338 trimers and tetramers. Based on the thermodynamic data shown in Table A3, the dominant fraction
339 of neutral monomers is hydrated (79% at RH=38% and 94% at RH=90%) while the fraction of
340 monomers containing NH₃ is negligible (0.02% at [NH₃]=0.3 ppb and 0.2% at [NH₃]=3 ppb,
341 RH=38%). As a result of the growing binding strength of NH₃ with the cluster size (Table A3),
342 the fraction of neutral sulfuric acid dimers containing one NH₃ molecule reaches 18% at
343 [NH₃]=0.3 ppb and 69% at [NH₃]=3 ppb when T=292 K and RH=38%. In the case of H₂SO₄
344 trimers and tetramers, data shown in Figure 3d are limited to the relative abundance of unhydrated
345 clusters only. Under the given conditions, most of trimers contain two NH₃ molecules while most
346 tetramers contain 3 NH₃ molecules. At [NH₃]=3 ppb, ~2% of trimers contain three NH₃ molecules
347 (i.e., $s=a=3$) and 55% of tetramers contain four NH₃ molecules (i.e., $s=a=4$). As a result of a
348 significant drop of ΔG_{+A}^0 in the case, when a/s ratio exceeds one (Table A3), the fraction of neutral
349 clusters with $a=s+1$ are negligible. The cluster distributions clearly indicate that small sulfuric acid
350 clusters are still not fully neutralized by NH₃ even if [NH₃] is at ppb level; and that the degree of
351 neutralization (i.e., $a:s$ ratio) increases with the cluster size.

352

353 2.4.2 Mean stepwise and accumulative Gibbs free energy change and impact of ammonia

354 In the TIMN model, the equilibrium distributions are used to calculate number concentrations
355 weighted stepwise Gibbs free energy change for adding one H₂SO₄ molecule to form a neutral,
356 positively charged, and negatively charged cluster containing s H₂SO₄ molecules ($\overline{\Delta G}_{s-1,s}$):

$$357 \quad \overline{\Delta G}_{s-1,s}^{+,-,0} = \sum_{a,w} f_{s,a,w}^{+,-,0} \Delta G_{s-1,s,a,w}^{+,-,0} \quad (9)$$

358 where $f_{s,a,w}^{+,-,0}$ is the equilibrium fraction of a particular cluster within a cluster type as shown in
359 Fig. 3.

360 In the atmosphere, where substantial nucleation is observed, the sizes of critical clusters are
361 generally small ($s < \sim 5-10$) (e.g., Sipilä et al., 2010) and nucleation rates are largely controlled by
362 the stability (or γ) of small clusters with $s < \sim 5-10$. QC calculations and experimental data on
363 clustering thermodynamics available for clusters of small sizes (Tables A2–A4), are critically
364 important as the formation of these small clusters is generally the limiting step for nucleation.
365 Nevertheless, thermodynamics data for larger clusters are also needed to develop a robust
366 nucleation model that can calculate nucleation rates under various conditions. Both measurements
367 and QC calculations (Tables A2–A4) show significant effects of charge and charge signs (i.e.,
368 positive or negative) on the stability and composition of small clusters. These charge effects
369 decrease quickly as the clusters grow, due to the short-ranged nature of dipole-charge interaction
370 and the quick decrease of electrical field strength around charged clusters as cluster sizes increase
371 (Yu, 2005). Based on experimental data (Kearle et al., 1967; Davidson et al., 1977; Wlodek et
372 al., 1980; Holland and Castleman, 1982; Froyd and Lovejoy, 2003), the stepwise ΔG values for
373 clusters decreases exponentially as the cluster sizes increase and approaches to the bulk values
374 when clusters containing more than $\sim 8-10$ molecules (Yu, 2005). Cluster compositions measured
375 with an atmospheric pressure interface time-of-flight (APi-TOF) mass spectrometer during
376 CLOUD experiments also show that the difference in the composition of positively and negatively
377 charged clusters quickly decreases as the number of H₂SO₄ molecules increases from 1 to ~ 10 and
378 exhibits little further changes (Schobesberger et al., 2015).

379 In the present TIMN model, we assume that both neutral and charged clusters have the same
380 composition when $s \geq 10$ and the following extrapolation scheme is used to calculate $\Delta G_{s-1,s}$ for
381 clusters up to $s=10$:

$$382 \quad \Delta G_{s-1,s} = \Delta G_{s_1-1,s_1} + \frac{\left(\Delta G_{s_2-1,s_2} - \Delta G_{s_1-1,s_1} \right) \left(e^{-s_2 c} - e^{-s_1 c} \right)}{\left(e^{-s_2 c} - e^{-s_1 c} \right)} \quad (10)$$

383 where $\Delta G_{s_1-1,s_1}$ is the stepwise mean Gibbs free energy change for H₂SO₄ addition for a specific
384 type (neutral, positive, or negative) of clusters at $s=s_1$ that can be derived from QC calculation
385 and/or experimental measurements, and $\Delta G_{s_2-1,s_2}$ is the corresponding value for clusters at $s=s_2$
386 ($=10$ in the present study) that is calculated in the capillarity approximation accounting for the
387 Kelvin effect. c in Eq. 10 is the exponential coefficient that determines how fast $\Delta G_{s-1,s}$
388 approaches to bulk values as s increases. In the present study, c is estimated by fitting $\Delta G_{s-1,s}$ at
389 $s=2$ and $s=3$ based on Eq. (10) to those from experimental (Hanson and Lovejoy, 2006; Kazil et
390 al., 2007) or quantum-chemical data (Table A3). Apparently the interpolation approximation Eq.
391 (10) is subject to uncertainty. Nevertheless, it is a reasonable approach to connect thermochemical
392 properties of QC data for small binary and ternary clusters that cannot be adequately described by
393 the capillarity approximation with those for large clusters that can be adequately described the very
394 same capillarity approximation, and is the best approach we can come up with at this point in order
395 to develop a model that can be applied to all conditions. Further QC and experimental studies of
396 the thermodynamics of relatively larger clusters can help to reduce the uncertainty.

397 For clusters with $s \geq s_2$, the capillarity approximation is used to calculate $\Delta G_{s-1,s}$ as

$$398 \quad \Delta G_{s-1,s} = -RT \ln(P/P_s) + \frac{2\sigma v_1 N_A}{r_s} \quad (11)$$

399 where P is the H₂SO₄ vapor pressure and P_s is the H₂SO₄ saturation vapor pressure over a flat
400 surface with the same composition as the cluster. σ is the surface tension and v_1 is the volume of
401 one H₂SO₄ molecule. r_s is the radius of the cluster and N_A is the Avogadro's number.

402 The scheme to calculate bulk $\Delta G_{s-1,s}$ ($s \geq 10$) for H₂SO₄-H₂O binary clusters has been
403 described in Yu (2007). For ternary nucleation, both experiments (Schobesberger et al., 2015) and
404 QC calculations (Table A4) indicate that the growth of relatively large clusters follows the $s=a$
405 line (i.e, in the composition of ammonia bisulfate). In the present TIMN model, the bulk $\Delta G_{s-1,s}$
406 values for ternary clusters are calculated based on parameterized H₂SO₄ saturation vapor pressure
407 over ammonia bisulfate as a function of temperature, derived by Martin et al. (1997) from vapor
408 pressures measured at temperature between 27 °C and °60 C, and surface tension measured at 298
409 K from Hyvarinen et al. (2005). The uncertainty in saturation vapor pressures and surface tension

410 used in the calculation of the bulk $\Delta G_{s-1,s}$ values is another source of uncertainty in the TIMN
411 model, although it is likely to be small compared to other uncertainties as the nucleation is
412 generally limited by the formation of small clusters.

413 Figure 4 presents stepwise ($\overline{\Delta G}_{s-1,s}$) and cumulative (total) $\overline{\Delta G}_s$ Gibbs free energy changes
414 associated with the formation of neutral, positively charged, and negatively charged binary and
415 ternary clusters containing s H_2SO_4 molecules under the conditions specified in the figure caption.
416 The clusters are assumed to be in equilibrium with water (Yu, 2007) and ammonia (Fig. 3). As
417 seen from Fig. 4, the presence of NH_3 reduces the mean $\overline{\Delta G}_{s-1,s}$ for larger clusters, which can be
418 treated as the bulk binary H_2SO_4 - H_2O solution (Schobesberger et al., 2015), by $\sim 3 \text{ kcal mol}^{-1}$,
419 indicating a substantial reduction in the H_2SO_4 vapor pressure over ternary solutions (Marti et al.,
420 1997). The comparison also shows that the influence of NH_3 on $\overline{\Delta G}_{s-1,s}$ of small clusters ($s \leq \sim 4$)
421 is much lower than that on larger ones and bulk solutions. For example, at $[\text{NH}_3]=0.3 \text{ ppb}$, the
422 differences in $\overline{\Delta G}_{s-1,s}$ between binary and ternary positive ions with $s=1$ and neutral clusters with
423 $s=2$ are only $0.45 \text{ kcal mol}^{-1}$ and $\sim 1 \text{ kcal mol}^{-1}$, respectively. In the case of negative ions, zero
424 and $0.27\text{--}0.45 \text{ kcal mol}^{-1}$ differences at $s \leq 2$ and $s=3\text{--}4$, respectively, were observed. The reduced
425 effect of ammonia on smaller clusters is explained (Tables A2-A4) by ammonia's weaker bonding
426 to smaller clusters than to larger ones, which in turn yields lower average NH_3 to H_2SO_4 ratios
427 (Fig. 3). It should be noted that QC data for positively charged clusters are very limited and the
428 interpolation approximation is subject to large uncertainty. In order for the nucleation on positive
429 ions to occur, the first step is for H_2SO_4 to attach to a positive ion that does not contain H_2SO_4 .
430 Unlike negative ions, the effect of charge on the bonding of H_2SO_4 with positive ions is much
431 weaker and thus the stepwise Gibbs free energy change for the addition of one H_2SO_4 molecule to
432 form a positively charged cluster is likely to be similar to that of neutral clusters, i.e., decreasing
433 with cluster size. Therefore, the QC data for positively charged clusters containing one H_2SO_4
434 molecule provides a critical constrain. The success of the model in predicting the $[\text{NH}_3]$ needed
435 for nucleation on positive ions to occur (see Section 3) show the usefulness of the first step data
436 and approximation.

437 As seen from Fig. 4, bonding of H_2SO_4 to small negatively charged clusters ($s < 3$) is much
438 stronger than that to neutrals and positive ions. As a result, at $s < 3$ the formation of negatively
439 charged clusters is barrierless ($\overline{\Delta G}_{s-1,s} < 0$). These small clusters cannot be considered as nucleated

440 particles because $\overline{\Delta G}_{s-1,s}$ (Fig. 4a) first increases and then decreases with growing s , reaching the
441 maximum barrier values at $s = \sim 3 - 6$. $\overline{\Delta G}_{s-1,s}$ can become positive for larger clusters due to the
442 charge effect decreasing quickly as the clusters are growing. The effect of NH_3 on negative ions
443 becomes important at $s \geq \sim 4$, when bonding between the clusters and NH_3 becomes strong enough
444 to contaminate a large fraction of binary clusters with ammonia (Fig. 3). In contrast, the impact of
445 NH_3 on neutral dimers and positively charged monomers of H_2SO_4 , as well as on $\overline{\Delta G}_{s-1,s}$ for both
446 positively charged and neutral clusters, monotonically decreases for all s , including $s \leq 5$.

447 $\overline{\Delta G}_{s-1,s}$ for charged and neutral clusters converge into the bulk values at $s \sim 10$, when impact
448 of the chemical identity of the core ion on the cluster composition becomes diffuse (Schobesberger
449 et al., 2015) and when the contribution of the electrostatic effect to $\overline{\Delta G}_{s-1,s}$ becomes less than \sim
450 $0.5 \text{ kcal mol}^{-1}$. The comparison of cumulative (total) $\overline{\Delta G}_s$ (Fig. 4b) indicates the lowest nucleation
451 barrier for the case of negative ions, followed by positive ions and neutrals. The barrierless
452 formation of clusters with s ranging from 1 to 3 substantially reduces the nucleation barrier for
453 negatively charged ions and facilitates their nucleation. The presence of 0.3 ppb of NH_3 lowers the
454 nucleation barrier for negative, positive and neutral clusters from $\sim 17, 24$ and 38 kcal mol^{-1} to 2,
455 7 and 16 kcal mol^{-1} , respectively. A relatively low nucleation barrier for charged ternary clusters
456 is explained by the simultaneous effect of ionization and NH_3 which also reduces the size of the
457 critical cluster (s^*).

458 It is important to note that the size of the critical cluster, commonly used to “measure” the
459 activity of nucleation agents in the classical nucleation theory (Coffman and Hegg, 1995;
460 Korhonen et al., 1999; Vehkamäki et al., 2002; Napari et al., 2002; Hamill et al., 1982) is no longer
461 a valid indicator, when charged molecular clusters and small nanoparticles are considered. As seen
462 from Fig. 4, positively charged ternary critical clusters ($s^*=3-4$) are smaller than the corresponding
463 negatively charged ones ($s^*=4-5$); however, the nucleation barrier for ternary positive clusters
464 under the condition specified in the figure caption is more than three times higher than that for
465 ternary negatives ones.

466

467 2.4.3 Size- and composition- dependent H_2SO_4 evaporation rates

468 As we mentioned earlier, H_2SO_4 is the key atmospheric nucleation precursor driving the
469 formation and growth of clusters in the ternary $\text{H}_2\text{SO}_4\text{-H}_2\text{O-NH}_3$ system while ions, H_2O , and
470 NH_3 act to stabilize the H_2SO_4 clusters. The clustering thermodynamic data derived from QC

471 calculations and measurements (Section 2.3) are used to constrain size- and composition-
 472 dependent Gibbs free energy changes and evaporation rates of H₂SO₄ which are critically
 473 important. Average or effective rates of H₂SO₄ molecule evaporation from positively charged,
 474 negatively charged, and neutral clusters containing s H₂SO₄ molecules ($\bar{\gamma}_s^{+,-,0}$) are calculated from
 475 $\bar{\Delta G}_{s-1,s}$ as:

$$476 \quad \bar{\gamma}_s^{+,-,0} = \beta_{s-1}^{+,-,0} N^0 \exp\left(\frac{\bar{\Delta G}_{s-1,s}}{RT}\right) \quad (12)$$

477 where N^0 is as defined in Eq. (7). The present model assumes only a single H₂SO₄ molecule
 478 evaporates, i.e. no water ligands, for instance, are attached to it. This is likely the dominant
 479 evaporation pathway as hydrated H₂SO₄ molecules are generally more stable.

480 Figure 5 gives the mean evaporation rate ($\bar{\gamma}$) of an H₂SO₄ molecule from these clusters under
 481 the conditions corresponding to Fig. 4. The shapes of $\bar{\gamma}$ curves are similar to those of $\bar{\Delta G}_{s-1,s}$ (Fig.
 482 4a) as $\bar{\gamma}$ values are largely controlled by $\bar{\Delta G}_{s-1,s}$ (Eq. 12). The presence of ammonia, as expected,
 483 significantly reduces the vapor pressure of H₂SO₄ over bulk aerosol (Marti et al., 1997), and,
 484 hence, the H₂SO₄ evaporation rate. The evaporation rates of both neutral and positive clusters
 485 decrease as s increases, and the positive clusters are uniformly more stable than corresponding
 486 neutral clusters. $\bar{\gamma}$ for negative ions first increases and then decreases as s increases, peaking
 487 around $s \sim 3 - 6$. The presence of NH₃ reduces the evaporation rates of larger clusters by more
 488 than two orders of magnitude and the effect decreases for smaller clusters, as the binding of NH₃
 489 to small neutral and charged clusters are weaker compared to that for larger clusters (Fig. 4). [NH₃]
 490 influences the average NH₃:H₂SO₄ ratio (Fig. 3) and the evaporation rates of these small clusters.
 491 The nucleation rates, limited by formation of small clusters ($s < \sim 5$), depend strongly on the
 492 stability or evaporation rate of these small clusters. While the binding of NH₃ to small neutral and
 493 charged clusters is weaker compared to that to larger clusters, small clusters containing NH₃ are
 494 much more stable than those without (Fig. 4) and thus ammonia is important for nucleation.

495 496 **3. TIMN rates and comparisons with CLOUD measurements**

497 The evolution of cluster/particle size distributions can be obtained by solving the dynamic
 498 equations 1-6. Since the concentrations of clusters of all sizes are predicted, the nucleation rates in
 499 the kinetic model can be calculated for any cluster size larger than the critical size of neutral
 500 clusters ($i > i^*$) (Yu, 2006b),

$$501 \quad J_i = J_i^+ + J_i^- + J_i^0 = \beta_{i,1}^+ N_1^0 N_i^+ - \gamma_i^+ N_{i+1}^+ + \beta_{i,1}^- N_1^0 N_i^- - \gamma_i^- N_{i+1}^- + \beta_{i,1}^0 N_1^0 N_i^0 - \gamma_i^0 N_{i+1}^0 \quad (13)$$

502 where J_i^+ , J_i^- , and J_i^0 are nucleation rates associated with positive, negative, and neutral clusters
503 containing i H₂SO₄ molecules. As a result of scavenging by pre-existing particles or wall loss, the
504 steady state J_i decreases as i increases. To compare with CLOUD measurements, we calculate
505 nucleation at cluster mobility diameter of 1.7 nm ($J_{1.7}$).

506 Many practical applications require information on the steady state nucleation rates. For each
507 nucleation case presented in this paper, constant values of [H₂SO₄] (i.e., N_1^0), [NH₃], T, RH, Q,
508 and $L_i^{+, -, 0}$ are assumed. The pre-existing particles with fixed surface area or wall loss serve as a
509 sink for all clusters. Under a given condition, cluster distribution and nucleation rate reach steady
510 state after a certain amount of time. We calculate size-dependent coefficients for a given case, and
511 then solve equations (1-6) to obtain the steady state cluster distribution and nucleation rate, with
512 the approach described in Yu (2006b).

513 Figure 6 shows a comparison of the model TIMN rates $J_{1.7}$ with CLOUD measurements, as a
514 function of [NH₃] under two ionization rates. It should be noted that Dunne et al. (2016) developed
515 a simple empirical parameterization (denoted thereafter as “CLOUDpara”) of binary, ternary and
516 ion-induced nucleation rates in CLOUD measurements as a function of [NH₃], [H₂SO₄], T, and
517 negative ion concentration. The predictions of CLOUDpara (Dunne et al., 2016) and ACDC based
518 on nucleation thermochemistry obtained using RI-CC2//B3LYP method (McGrath et al., 2012;
519 Kurten et al., 2016) are also presented in Fig. 6 for comparisons.

520 Like the CLOUD measurements, the TIMN predictions reveal a complex dependence of $J_{1.7}$
521 on [NH₃], and an analysis of the TIMN results shows this behavior can be explained by the
522 differing responses of negative, positive and neutral clusters to the presence of ammonia (Fig. 4).
523 Under the conditions specified in Fig. 6, nucleation is dominated by negative ions for [NH₃] < ~0.5
524 ppb, by both negative and positive ions for [NH₃] from ~0.5 ppb to ~10 ppb (with background
525 ionization), or ~20 ppb (with pion-enhanced ionization), and by neutrals at higher [NH₃].
526 According to TIMN, [NH₃] of at least 0.6–1 ppb are needed before positive ions contribute
527 significantly to nucleation rates – in good agreement with the threshold found in the CLOUD
528 experiments (Kirkby et al., 2011; Schobesberger et al., 2015). TIMN simulations also extend
529 CLOUD data at [NH₃] of ~1 ppb to include a “zero-sensitivity zone” in the region of 1-10 ppb,
530 followed by a region of strong sensitivity of $J_{1.7}$ to [NH₃] commencing at [NH₃] > ~10-20 ppb. The
531 latter zone may have important implications for NPF in heavily polluted regions, including much
532 of India and China, where [NH₃] may exceed 10-20 ppb (Behera and Sharma, 2010; Meng et al.,
533 2017). It is noteworthy in Fig. 6 that the dependence of $J_{1.7}$ on [NH₃] and Q predicted by the ACDC
534 model (McGrath et al., 2012) and the CLOUD data parameterization (Dunne et al., 2016) deviate

535 substantially from the experimental data as well as the TIMN simulations. The CLOUDpara does
536 not consider impacts of positive ions and such key controlling parameters as RH and surface area
537 of pre-existing particles. Dunne et al. (2016) reported that CLOUDpara is also very sensitive to
538 the approach to parameterize T dependence, showing that the contribution of ternary ion-induced
539 nucleation to NPF below 15 km altitude has grown from 9.6% to 37.5%, after the initial empirical
540 temperature function was replaced with a simpler one.

541 Figure 7 presents a more detailed comparison of TIMN simulations with CLOUD
542 measurements of $J_{1.7}$ as a function of $[\text{H}_2\text{SO}_4]$, T, and RH. The TIMN model reproduces both the
543 absolute values of $J_{1.7}$ and its dependencies on $[\text{H}_2\text{SO}_4]$, T, and RH, in a wide range of
544 temperatures ($T=208 - 292$ K) and $[\text{H}_2\text{SO}_4]$ ($5 \times 10^5 - 5 \times 10^8 \text{ cm}^{-3}$). As expected, nucleation rates
545 are very sensitive to $[\text{H}_2\text{SO}_4]$ and T. For example, $J_{1.7}$ increases by three to five orders of magnitude
546 with an increase in $[\text{H}_2\text{SO}_4]$ of a factor of 10, and by roughly one order of magnitude for a
547 temperature decrease of 10 degree, except in cases where the nucleation rate is limited by Q (for
548 example, $[\text{H}_2\text{SO}_4] \approx 10^8 - 10^9 \text{ cm}^{-3}$ at $T=278$ K and 292 K, shown in Fig. 7a). The key difference
549 between CLOUDpara and TIMN predictions is that $\text{dln}J_{1.7}/\text{dln}[\text{H}_2\text{SO}_4]$ ratio predicted by
550 CLOUDpara is nearly constant while TIMN shows that this ratio depends on both $[\text{H}_2\text{SO}_4]$ and T.
551 The CLOUD measurements taken at $T=278$ K clearly show (in agreement with the TIMN) that
552 $\text{dln}J_{1.7}/\text{dln}[\text{H}_2\text{SO}_4]$ is not constant. CLOUDpara overestimates $J_{1.7}$ compared to both
553 measurements and TIMN simulations, except for the case, when $T=278$ K and $[\text{H}_2\text{SO}_4]$ ranges
554 from $\sim 7 \times 10^6$ to $5 \times 10^7 \text{ cm}^{-3}$, with deviation of CLOUDpara from experimental data and TIMN
555 growing with the lower temperature.

556 Both CLOUD measurements and TIMN simulations (Fig. 7b) show an important influence of
557 RH on nucleation rates. In particular, CLOUD measurements indicate 1-5 order of magnitude rise
558 in $J_{1.7}$ after RH increases from 10% to 70-80% and a stronger effect of RH on nucleation rates at
559 higher temperatures under the conditions shown in Fig. 7b. The RH dependence of $J_{1.7}$ predicted
560 by the TIMN model is consistent with measurements, being slightly weaker than the measured at
561 high RH.

562 Figure 8 compares TIMN model predictions with all 377 data points of CLOUD measurements
563 reported in data Table S1 of Dunne et al. (2016). The vertical error bars show the range of J_{model}
564 associated with the uncertainty in the $[\text{H}_2\text{SO}_4]$ measured (-50%, +100%). The effect of uncertainty
565 in measured $[\text{NH}_3]$ (-50%, +100%) is not included. At the presence of ionization (Fig. 8a), J_{model}
566 agrees with CLOUD measurements within the uncertainties under mainly all conditions, although
567 J_{model} tends to be slightly lower than J_{obs} when $T=292 - 300$ K and J_{obs} is relatively small ($< \sim 1 \text{ cm}^{-3} \text{ s}^{-1}$).
568 For the neutral nucleation (Fig. 8b), the model agrees well with observations at low T ($T=205$
569 $- 223$ K) but deviates from observations as T increases. The under-prediction of the model for
570 neutral nucleation at $T=278 - 300$ K cannot be explained by the uncertainties in measured $[\text{H}_2\text{SO}_4]$

571 and [NH₃]. Apparently for neutral nucleation the model predicts much stronger temperature
572 dependence than the CLOUD measurements. The possible reasons for the difference include the
573 uncertainties in both the model (especially the thermodynamics data and approximation) and
574 measurements. It should be noted that, under the conditions of high T and absence of ions, the role
575 of cluster evaporation (i.e. thermodynamics) becomes more important (i.e. higher evaporation
576 and/or generally less tightly bound clusters) and the effect of the possible biases of the used
577 thermochemistry can be more clearly revealed. The contamination (by amines) in the CLOUD
578 measurements (Kirkby et al., 2011) can be another possible reason. The level of contamination in
579 the cloud chamber appears to increase with temperature (Kurten et al., 2016), which may explain
580 the good agreement at low T and increased deviation at higher T. Further research is needed to
581 identify the source of the difference for neutral ternary nucleation at high T.

582

583 **4. Summary**

584 A comprehensive kinetically-based H₂SO₄-H₂O-NH₃ ternary ion-mediated nucleation (TIMN)
585 model, constrained with thermodynamic data from quantum-chemical calculations and laboratory
586 measurements, has been developed and used to shed a new light on physico-chemical processes
587 underlying the effect of ammonia on NPF. We show that the stabilizing effect of NH₃ grows with
588 the cluster size, and that the reduced effect of ammonia on smaller clusters is caused by weaker
589 bonding that in turn yields lower average NH₃ to H₂SO₄ ratios. NH₃ was found to impact nucleation
590 barriers for neutral, positively charged, and negatively charged clusters differently due to the large
591 difference in the binding energies of NH₃, H₂O, and H₂SO₄ to small clusters of different charging
592 states. The lowest and highest nucleation barriers are observed in the case of negative ions and
593 neutrals, respectively. Therefore, nucleation of negative ions is favorable, followed by nucleation
594 of positive ions and neutrals. Different responses of negative, positive and neutral clusters to
595 ammonia result in a complex dependence of ternary nucleation rates on [NH₃]. The TIMN model
596 reproduces both the absolute values of nucleation rates and their dependencies on the key
597 controlling parameters and agrees with the CLOUD measurements for all the cases at the presence
598 of ionization. For the neutral ternary nucleation, the model agrees well with observations at low
599 temperature but deviates from observations as temperature increases.

600 The TIMN model developed in the present study may subject to uncertainties associated with
601 the uncertainties in thermodynamic data and interpolation approximation for pre-nucleation
602 clusters. Further measurements and quantum calculations, especially for relatively larger clusters,
603 are needed to reduce the uncertainties. While the TIMN model predicts nucleation rates in a good
604 overall agreement with the CLOUD measurements, its ability to explain the NPF events observed
605 in the real atmosphere is yet to be quantified and will be investigated in further studies.

606

607 Appendix

608 A1. Quantum-chemical studies of neutral and charged binary and ternary clusters

609 Thermochemical data for small neutral and charged binary $\text{H}_2\text{SO}_4\text{-H}_2\text{O}$ and ternary $\text{H}_2\text{SO}_4\text{-}$
610 $\text{H}_2\text{O-NH}_3$ clusters has been reported in a number of earlier publications (Bandy and Ianni, 1998;
611 Ianni and Bandy, 1999; Torpo et al., 2007; Nadykto et al., 2008; Herb et al., 2011, 2013; Temelso
612 et al., 2012a, b; DePalma et al., 2012; Ortega et al., 2012; Chon et al., 2014; Husar et al., 2014;
613 Henschel et al., 2014, 2016; Kurten et al., 2015). The PW91PW91/6-311++G(3df,3pd) method,
614 which is a combination of the Perdue-Wang PW91PW91 density functional with the largest Pople
615 6-311++G(3df,3pd) basis set, has thoroughly been validated and agrees well with existing
616 experimental data. In earlier studies, this method has been applied to a large variety of
617 atmospherically-relevant clusters (Nadykto et al. 2006, 2007a, b, 2008, 2014, 2015; Torpo et al.
618 2007; Zhang et al., 2009; Elm et al. 2012; Leverentz et al. 2013; Xu and Zhang, 2012; Xu and
619 Zhang, 2013; Elm et al., 2013; Zhu et al. 2014; Bork et al. 2014; Elm and Mikkelsen, 2014; Peng
620 et al. 2015; Miao et al 2015; Chen et al., 2015; Ma et al., 2016) and has been shown to be well
621 suited to study the $\text{H}_2\text{SO}_4\text{-H}_2\text{O}$ and $\text{H}_2\text{SO}_4\text{-H}_2\text{O-NH}_3$ clusters, as evidenced by a very good
622 agreement of the computed values with measured cluster geometries, vibrational fundamentals,
623 dipole properties and formation Gibbs free energies (Nadykto et al., 2007a, b, 2008, 2014, 2015;
624 Herb et al., 2013; Elm et al., 2012, 2013; Leverentz et al., 2013; Bork et al., 2014) and with high
625 level ab initio results (Temelso et al., 2012a, b; Husar et al., 2012; Bustos et al., 2014).

626 We have extended the earlier QC studies of binary and ternary clusters to larger sizes. The
627 computations have been carried out using Gaussian 09 suite of programs (Frisch et al., 2009). In
628 order to ensure the quality of the conformational search we have carried out a thorough sampling
629 of conformers. We have used both basin hopping algorithm, as implemented in Biovia Materials
630 Studio 8.0, and locally developed sampling code. The sampling code is based on the following
631 principle: mesh, with molecule to be added to the cluster placed in the mesh nodes, is created
632 around the cluster, and blind search algorithm is used to generate the guess geometries. The mesh
633 density and orientation of molecules are variable, as well as the minimum distance between
634 molecules and cluster. Typically, for each cluster of a given chemical composition a thousand to
635 several thousands of isomers have been sampled. We used a three-step optimization procedure,
636 which includes (i) pre-optimization of initial/guess geometries by semi-empirical PM6 method,
637 separation of the most stable isomers located within 15 kcal mol^{-1} of the intermediate global
638 minimum and duplicate removal, followed by (ii) optimization of the selected isomers meeting the
639 aforementioned stability criterion by PW91PW91/CBSB7 method and (iii) the final optimization
640 of the most stable at PW91PW91/CBSB7 level isomers within 5 kcal mol^{-1} of the current global
641 minimum using PW91PW91/6-311++G(3df,3pd) method. Typically, only ~4-30% of initially
642 sampled isomers reach the second (PW91PW91/CBSB7) level, where ~10-40% of isomers

643 optimized with PW91PW91/CBSB7 are selected for the final run. Typically, the number of
644 equilibrium isomers of hydrated clusters is larger than that of unhydrated ones of similar chemical
645 composition. Table A1 shows the numbers of isomers converged at the final PW91PW91/6-
646 311++G(3df,3pd) optimization step for selected clusters and HSG values of the most stable
647 isomers used in the present study. The number of isomers optimized at the PW91PW91/6-
648 311++G(3df,3pd) level of theory varies from case to case, typically being in the range of ~10-200.

649 The computed stepwise enthalpy, entropy, and Gibbs free energies of cluster formation have
650 been thoroughly evaluated and used to calculate the evaporation rates of H₂SO₄ from neutral,
651 positive and negative charged clusters.

652

653 A1.1 Positively charged clusters

654 Table A2 presents the computed stepwise Gibbs free energy changes under standard conditions
655 (ΔG°) for positive binary and ternary clusters, along with the corresponding experimental data or
656 semi-experimental estimates. Figure 2 in the main text shows ΔG associated with the addition of
657 water (ΔG_{+W}°), ammonia (ΔG_{+A}°), and sulfuric acid (ΔG_{+S}°) to binary and ternary clusters as a
658 function of the cluster hydration number w . Both the absolute values and trends in ΔG_{+W}° derived
659 from calculations are in agreement with the laboratory measurements within the uncertainty range
660 of ~1-2 kcal mol⁻¹ for both QC calculations and measurements. This confirms the efficiency and
661 precision of QC methods in calculating thermodynamic data needed for the development of
662 nucleation models. Nevertheless, it should be noted that the uncertainties in computed free energies
663 of 1-2 kcal mol⁻¹ may lead to large uncertainty in predicted particle formation rates. By increasing
664 or decreasing all Gibbs free energies by 1 kcal mol⁻¹, Kürten et al. (2016) showed that, depending
665 on the conditions, the modeled particle formation rate can change from less than an order of
666 magnitude to several orders of magnitude. Uncertainties estimated by Kürten et al. (2016)
667 represent the upper limit because computed free energies may be overestimated for some clusters
668 and underpredicted for others that leads to partial or, in some case, full error cancelation.

669

670 A1.2 Neutral clusters

671 Table A3 presents the computed stepwise Gibbs free energy changes for the formation of
672 ternary S_sA_aW_w clusters under standard conditions. The corresponding binary electrically neutral
673 clusters can be found in previous publications (e.g., Nadykto et al., 2008; Herb et al., 2011). The
674 thermodynamic properties of the S₁A₁ have been reported in a number of computational studies
675 (e.g., Herb et al., 2011; Kurten et al., 2007; Nadykto and Yu, 2007). However, most of these
676 studies, except for Nadykto and Yu (2007) and Henschel et al. (2014; 2016), did not consider the
677 impact of H₂O on cluster thermodynamics. We have extended the earlier studies of Nadykto and
678 Yu (2007) and Herb et al. (2011) to larger clusters up to S₄A₅ (no hydration) and up to S₂A₂

679 (hydration included). The free energy of binding of NH₃ to H₂SO₄ (or H₂SO₄ to NH₃) obtained
680 using our method is -7.77 kcal mol⁻¹ that is slightly more negative than values reported by other
681 groups (-6.6 – -7.61 kcal mol⁻¹) and within less than 0.5 kcal mol⁻¹ of the experimental value of -
682 8.2 kcal mol⁻¹ derived from CLOUD measurements (Kurten et al., 2015).

683 As it may be seen from Table A3, the NH₃ binding to S₁₋₂W_w weakens as *w* increases. The
684 average ΔG_{+W}^0 for S₁W_w formation derived from a combination of laboratory measurements and
685 quantum chemical studies are -3.02, -2.37, and -1.40 kcal mol⁻¹ for the first, second, and third
686 hydration, respectively (Yu, 2007). This indicates that a large fraction of H₂SO₄ monomers in the
687 Earth's atmosphere is likely hydrated. Therefore, the decreasing NH₃ binding strength to hydrated
688 H₂SO₄ monomers implies that RH (and T) will affect the relative abundance of H₂SO₄ monomers
689 containing NH₃. Currently, no experimental data or observations are available to evaluate the
690 impact of hydration (or RH) on ΔG_{+A}^0 . Table A3 shows that the presence of NH₃ in H₂SO₄ clusters
691 suppress hydration and that ΔG_{+W}^0 for S₂A₂ falls below -2.0 kcal mol⁻¹. This is consistent with
692 earlier studies by our group (Herb et al., 2011) and others (Henschel et al., 2014, 2016) showing
693 that large S_nA_n clusters (*n*>2) are not hydrated under typical atmospheric conditions. In the present
694 study, the hydration of neutral S_nA_n clusters at *n*>2 is neglected, due to the lack of thermodynamic
695 data.

696 The number of NH₃ molecules in the cluster (or H₂SO₄ to NH₃ ratio) significantly affects ΔG_{+S}^0
697 and ΔG_{+A}^0 values. For example, ΔG_{+S}^0 for S₃A_a clusters increases from -7.08 kcal mol⁻¹ to -16.92
698 kcal mol⁻¹ and ΔG_{+A}^0 decreases from -16.14 kcal mol⁻¹ to -8.93 kcal mol⁻¹ as *a* is growing from 1
699 to 3. For S₄A_a clusters, ΔG_{+S}^0 is increasing from -7.48 kcal mol⁻¹ to -16.26 kcal mol⁻¹ and ΔG_{+A}^0
700 decreases from -17.16 kcal mol⁻¹ to -11.34 kcal mol⁻¹ as *a* increases from 2 to 4. ΔG_{+A}^0 for S₄A₁
701 cluster is by 1.38 kcal mol⁻¹ less negative than that for S₄A₂. ΔG_{+S}^0 for the S₄A₁ cluster is also quite
702 low (-4.16 kcal mol⁻¹) that might indicate the possible existence of a more stable S₄A₁ isomer,
703 which is yet to be identified. In the presence of NH₃, the uncertainty in the thermochemistry data
704 for S₄A₁ will not significantly affect ternary nucleation rates because most of S₄-clusters contain
705 3 or 4 NH₃ molecules.

706 For the S_sA_a clusters with *s*=*a*, ΔG_{+A}^0 increases as cluster is growing while ΔG_{+S}^0 first increases
707 significantly as S₁A₁ is converting into S₂A₂ and then levels off as S₂A₂ is converting into S₄A₄.
708 We also observe a significant drop in ΔG_{+A}^0 in the case when NH₃/H₂SO₄ ratio exceeds 1. This
709 finding is consistent with the ACDC model calculation showing that growth of neutral S_sA_a
710 clusters follows the *s*=*a* pathway (Schobesberger et al., 2015).

711

712 A1.3 Negative ionic clusters

713 Table A4 shows ΔG_{+W} , ΔG_{+A} , and ΔG_{+S} needed to form negatively charged clusters under
714 standard conditions, along with available semi-experimental values (Froyd and Lovejoy, 2003).

715 H₂O binding to negatively charged S⁻S_s clusters significantly strengthens with increasing *s*, from
 716 $\Delta G_{+W}^0 = -0.61$ to -1.83 kcal mol⁻¹ at *s*=1-2 to $\Delta G_{+W}^0 = -3.5$ kcal mol⁻¹ at *w*=1 and -2.25 kcal mol⁻¹ at
 717 *w*=4 at *s*=4. ΔG_{+W}^0 values at *s*=3 and 4 are slightly more negative (by $\sim 0.1 - 0.9$ kcal mol⁻¹) than
 718 those reported by Froyd and Lovejoy (2003). Just like H₂O binding, NH₃ binding to S⁻S_s at *s*<3 is
 719 very weak, with ΔG_{+A}^0 ranging from $+2.81$ kcal mol⁻¹ at *s*=0 to -4.85 kcal mol⁻¹ at *s*=2. However,
 720 it significantly increases as *s* is growing. In particular, at *s*≥3 ΔG_{+A}^0 is ranging from -11.89 kcal
 721 mol⁻¹ for S⁻S₃A₁ to -15.37 kcal mol⁻¹ for S⁻S₄A₁. NH₃ clearly cannot get into small negative ions.
 722 However, it can easily attach to larger negative ions with *s*≥3 that is consistent with CLOUD
 723 measurements (Schobesberger et al., 2015). Since hydration weakens NH₃ binding in S⁻S₃A₁W_w
 724 and S⁻S₄A₁W_w clusters, its impacts on the cluster formation and nucleation rates may potentially
 725 be important.

726 In contrast to H₂O and NH₃, binding of H₂SO₄ to small negative ions (*s*<3) is very strong.
 727 These ions are very stable even when they contain no NH₃ or H₂O molecules. High electron
 728 affinity of H₂SO₄ molecules results in the high stability of S⁻S_s at *s*=1-2. However, the charge
 729 effect reduces as *s* is growing. In particular, ΔG_{+S}^0 of S⁻S_s drops from -32.74 kcal mol⁻¹ at *s*=1 to
 730 -10.58 kcal mol⁻¹ and -8.28 kcal mol⁻¹ at *s*=3 and 4, respectively. At the same time, ΔG_{+A}^0 increases
 731 from 0.08 kcal mol⁻¹ (*s*=1) to -11.89 kcal mol⁻¹ (*s*=3) and -15.37 kcal mol⁻¹ (*s*=4). The hydration
 732 of S⁻S_s at *s*=3, 4 enhances the strength of H₂SO₄ binding, especially at *s*=4. ΔG_{+S}^0 values for S⁻S₃-
 733 ₄W_w are consistently $\sim 1.5 - 3$ kcal mol⁻¹ less negative than the corresponding semi-experimental
 734 estimates (Table A4). The possible reasons behind the observed systematic difference are yet to
 735 be identified and include the use of low-level *ab initio* HF method to compute reaction enthalpies
 736 and uncertainties in experimental enthalpies in studies by Froyd and Lovejoy (2003).

737 NH₃ binding to S⁻S₃ significantly enhances the stability of H₂SO₄ in the cluster by ~ 7 kcal mol⁻¹
 738 compared to ΔG_{+S}^0 for the corresponding binary counterpart. The binding of the second NH₃ to
 739 S⁻S₃A to form S⁻S₃A₂ is much weaker ($\Delta G_{+A}^0 = -7.27$ kcal mol⁻¹) than that of the first NH₃ molecule
 740 ($\Delta G_{+A}^0 = -11.89$ kcal mol⁻¹). This indicates that most of S⁻S₃A_a can only contain one NH₃ molecule,
 741 in a perfect agreement with the laboratory study of Schobesberger et al. (2015). In the case of S⁻
 742 S₄, binding of the first ($\Delta G_{+A}^0 = -15.37$ kcal mol⁻¹) and second (and -12.23 kcal mol⁻¹) NH₃
 743 molecules to the cluster is quite strong, while the attachment of NH₃ leads to substantial
 744 stabilization of H₂SO₄ in the cluster, as evidenced by ΔG_{+S}^0 growing from -8.28 kcal mol⁻¹ at *a*=0
 745 to -11.76 kcal mol⁻¹ and -16.71 kcal mol⁻¹ at *a*=1 and *a*=2, respectively. The NH₃ binding free
 746 energy to S⁻S₄A₂ (to form S⁻S₄A₃) drops to -7.59 kcal mol⁻¹, indicating, in agreement with the
 747 CLOUD measurements (Schobesberger et al., 2015) that most of S⁻S₄ clusters contain 1 or 2 NH₃
 748 molecules.

749

750 **Acknowledgments.** The authors thank Richard Turco (Distinguished Professor Emeritus, UCLA)
751 for comments that helped to improve the manuscript. This study was supported by NSF under
752 grant 1550816, NASA under grant NNX13AK20G, and NYSERDA under contract 100416. ABN
753 would like to thank the Russian Science Foundation and the Ministry of Science and Education of
754 Russia (under grants 1.6198.2017/6.7 and 1.7706.2017/8.9) for support and the Center of
755 Collective Use of MSTU Stankin for providing resources.

756
757 **Data availability.** All relevant data are available in the article, or from the corresponding authors
758 upon request.

759 **References**

- 761 Almeida, J., et al., Molecular understanding of sulphuric acid–amine particle nucleation in the
762 atmosphere, *Nature*, 502, 359-363, 2013.
- 763 Ball, S. M., Hanson, D. R., Eisele, F. L., and McMurry, P. H., Laboratory studies of particle
764 nucleation: Initial results for H₂SO₄, H₂O, and NH₃ vapors, *J. Geophys. Res.*, 104, 23709-23718,
765 10.1029/1999JD900411, 1999.
- 766 Bandy, A.R. and Ianni, J.C., Study of the hydrates of H₂SO₄ using density functional theory. *The*
767 *Journal of Physical Chemistry A*, 102(32), pp.6533-6539, 1998.
- 768 Behera, S. N., and M. Sharma, Investigating the potential role of ammonia in ion chemistry of fine
769 particulate matter formation for an urban environment, *The Science of the Total Environment*,
770 408(17), 3569-3575, 2010.
- 771 Benson, D. R., M. E. Erupe, and S.-H. Lee, Laboratory-measured H₂SO₄-H₂O-NH₃ ternary
772 homogeneous nucleation rates: Initial observations, *Geophys. Res. Lett.*, 36, L15818,
773 doi:10.1029/2009GL038728, 2009.
- 774 Bork, N., Du, L., Reiman, H., Kurtén, T. and Kjaergaard, H.G., Benchmarking ab initio binding
775 energies of hydrogen-bonded molecular clusters based on FTIR spectroscopy, *Journal of*
776 *Physical Chemistry A*, 118(28), 5316-5322, 2014.
- 777 Bustos, D.J., Temelso, B. and Shields, G.C., Hydration of the Sulfuric Acid–Methylamine
778 Complex and Implications for Aerosol Formation. *The Journal of Physical Chemistry A*,
779 118(35), pp.7430-7441, 2014.
- 780 Butler, T., Vermeulen, F., Lehmann, C. M., Likens, G. E., & Puchalski, M.. Increasing ammonia
781 concentration trends in large regions of the USA derived from the NADP/AMoN network.
782 *Atmospheric Environment*, 146, 132–140. 2016.

783 Chen, M., M. Titcombe, J. Jiang, C. Kuang, M. L. Fischer, E. Edgerton, F. L. Eisele, J. I. Siepmann,
784 D. H. Hanson, J. Zhao, and P. H. McMurry, Acid-base chemical reaction model for nucleation
785 rates in the polluted boundary layer. *Proc. Nat. Acad. Sci.*, 109, 18713–18718, 2012.

786 Chon, N.L., Lee, S.H. and Lin, H., A theoretical study of temperature dependence of cluster
787 formation from sulfuric acid and ammonia. *Chemical Physics*, 433, pp.60-66, 2014.

788 Coffman, D. J., and Hegg, D. A., A preliminary study of the effect of ammonia on particle
789 nucleation in the marine boundary layer, *J. Geophys. Res.*, 100, 7147-7160, 1995.

790 Davidson, J. A., Fehsenfeld, F.C., Howard, C.J.: The heats of formation of NO_3^- and NO_3^-
791 association complexes with HNO_3 and HBr , *Int. J. Chem. Kinet.*, 9, 17, 1977.

792 Dawson M.L., et al., Simplified mechanism for new particle formation from methanesulfonic acid,
793 amines and water via experiments and ab initio calculations, *Proc Natl Acad Sci USA*
794 109:18719–18724, 2012.

795 DePalma, J.W., Bzdek, B.R., Doren, D.J. and Johnston, M.V., Structure and energetics of
796 nanometer size clusters of sulfuric acid with ammonia and dimethylamine, *Journal of Physical*
797 *Chemistry A*, 116(3), pp.1030-1040, 2012.

798 Doyle, G. J., Self-nucleation in the sulfuric acid-water system, *J. Chem. Phys.*, 35, 795–799, 1961.

799 Dunne, E. M., et al., Global particle formation from CERN CLOUD measurements, *Science*,
800 doi:10.1126/science.aaf2649, 2016.

801 Duplissy J., et al., Effect of ions on sulfuric acid-water binary particle formation: 2. Experimental
802 data and comparison with QC-normalized classical nucleation theory, *J. Geophys. Res. Atmos.*,
803 121, 1752–1775, doi:10.1002/2015JD023539, 2016.

804 Elm, J. and Mikkelsen, K.V., Computational approaches for efficiently modelling of small
805 atmospheric clusters, *Chemical Physics Letters*, 615, 26-29, 2014.

806 Elm, J., Bilde, M. and Mikkelsen, K.V., Assessment of binding energies of atmospherically
807 relevant clusters, *Physical Chemistry Chemical Physics*, 15(39), 16442-16445, 2013.

808 Elm, J., Bilde, M. and Mikkelsen, K.V., Assessment of density functional theory in predicting
809 structures and free energies of reaction of atmospheric prenucleation clusters, *Journal of*
810 *chemical theory and computation*, 8(6), 2071-2077, 2012.

811 Frisch, M. J., Trucks, G. W., Schlegel, H. B., Scuseria, G. E., Robb, M. A., Cheeseman, J. R.,
812 Scalmani, G., Barone, V., Mennucci, B., et al., *Gaussian 09*, Gaussian, Inc., Wallingford CT,
813 2009.

814 Froyd K. D., and Lovejoy E. R., Bond energies and structures of ammonia-sulfuric acid positive
815 cluster ions, *J. Phys. Chem. A*, 116(24), 5886–5899, doi:10.1021/jp209908f, 2012.

816 Froyd, K. D., and Lovejoy, E. R., Experimental thermodynamics of cluster ions composed of
817 H_2SO_4 and H_2O . 1. Positive ions, *J. Phys. Chem. A*, 107, 9800–9811, 2003.

818 Froyd, K. D., and Lovejoy, E. R., Experimental thermodynamics of cluster ions composed of
819 H₂SO₄ and H₂O. 2. Measurements and ab initio structures of negative ions, *J. Phys. Chem. A*,
820 107, 9812–9824, 2003.

821 Froyd, K. D., and Lovejoy, E. R., Experimental thermodynamics of cluster ions composed of
822 H₂SO₄ and H₂O. 1. Positive ions, *J. Phys. Chem. A*, 107, 9800–9811, 2003.

823 Froyd, K. D., Ion induced nucleation in the atmosphere: Studies of NH₃, H₂SO₄, and H₂O cluster
824 ions, Ph.D. thesis, Univ. of Colo., Boulder, 2002.

825 Glasoe, W. A., Volz, K., Panta, B., Freshour, N., Bachman, R., Hanson, D. R., McMurry, P. H.,
826 and Jen, C.. Sulfuric acid nucleation: An experimental study of the effect of seven bases. *Journal*
827 *of Geophysical Research: Atmospheres*, 120(5), 1933-1950, 2015.

828 Hamill, P., Turco, R. P., Kiang, C. S., Toon, O. B., & Whitten, R. C., An analysis of various
829 nucleation mechanisms for sulfate particles in the stratosphere. *Journal of Aerosol Science*, 13,
830 561–585, 1982.

831 Hanson, D. R., and F. Eisele, Diffusion of H₂SO₄ in humidified nitrogen: Hydrated H₂SO₄, *J. Phys.*
832 *Chem. A*, 104, 1715 – 1719, 2000.

833 Hanson, D. R., and F. L. Eisele, Measurement of prenucleation molecular clusters in the NH₃,
834 H₂SO₄, H₂O system, *J. Geophys. Res.*, 107(D12), 4158, doi:10.1029/2001JD001100, 2002.

835 Hanson, DR., Lovejoy, ER, Measurement of the thermodynamics of the hydrated dimer and
836 trimers, *J. Phys. Chem. A* 110: 9525-9538 DOI: 10.1021/jp062844w, 2006.

837 Henschel, H., J. C. A. Navarro, T. Yli-Juuti, O. Kupiainen-Määttä, T. Olenius, I. K. Ortega, S. L.
838 Clegg, T. Kurtén, I. Riipinen, and H. Vehkamäki, Hydration of atmospherically relevant
839 molecular clusters: Computational chemistry and classical thermodynamics, *J. Phys. Chem. A*,
840 118, 2599–2611, 2014.

841 Henschel, H., T. Kurtén, and H. Vehkamäki, Computational study on the effect of hydration on
842 new particle formation in the sulfuric acid/ammonia and sulfuric acid/dimethylamine systems,
843 *J. Phys. Chem. A*, 120, 1886–1896, doi:10.1021/acs.jpca.5b11366, 2016.

844 Herb, J., Y. Xu, F. Yu, and A. B. Nadykto, Large Hydrogen-Bonded Pre-Nucleation (HSO₄⁻
845)(H₂SO₄)_m(H₂O)_k and (HSO₄⁻)(NH₃)(H₂SO₄)_m(H₂O)_k Clusters in the Earth's Atmosphere, *J.*
846 *Phys. Chem., A*, 117, 133-152, DOI: 10.1021/jp3088435, 2013.

847 Herb., J., A. Nadykto, and F. Yu, Large Ternary Hydrogen-Bonded Pre-Nucleation Clusters in the
848 Earth's Atmosphere, *Chemical Physics Letters*, 518, 7-14, 10.1016/j.cplett.2011.10.035, 2011.

849 Holland, P. M., and Castleman, A. W., Jr.: Thomson equation revisited in light of ion-clustering
850 experiments, *J. Phys. Chem.*; 86, 4181-4188, 1982.

851 Hoppel, W.A., and G. M. Frick, Ion-aerosol attachment coefficients and the steady-state charge
852 distribution on aerosols in a bipolar ion environment, *Aerosol Sci. Tech.*, 1-21, 1986.

853 Husar, D.E., Temelso, B., Ashworth, A.L. and Shields, G.C., Hydration of the bisulfate ion:
854 atmospheric implications. *The Journal of Physical Chemistry A*, 116(21), pp.5151-5163, 2012.

855 Hyvärinen, A., T. Raatikainen, A. Laaksonen, Y. Viisanen, and H. Lihavainen, Surface tensions
856 and densities of $\text{H}_2\text{SO}_4 + \text{NH}_3 + \text{water}$ solutions, *Geophys. Res. Lett.*, 32, L16806,
857 doi:10.1029/2005GL023268, 2005.

858 Ianni, J.C. and Bandy, A.R., A Density Functional Theory Study of the Hydrates of $\text{NH}_3\text{-H}_2\text{SO}_4$
859 and Its Implications for the Formation of New Atmospheric Particles. *The Journal of Physical*
860 *Chemistry A*, 103(15), pp.2801-2811, 1999.

861 Jacobson, M., Turco, R., Jensen, E. and Toon O.: Modeling coagulation among particles of
862 different composition and size, *Atmos. Environ.*, 28, 1327-1338, 1994.

863 Jolly, William L., *Modern Inorganic Chemistry (2nd Edn.)*. New York: McGraw-Hill. ISBN 0-07-
864 112651-1, 1991.

865 Kazil, J., Lovejoy, E. R., Jensen, E. J., and Hanson, D. R.: Is aerosol formation in cirrus clouds
866 possible?, *Atmos. Chem. Phys.*, 7, 1407-1413, <https://doi.org/10.5194/acp-7-1407-2007>, 2007.

867 Kebarle, P., S. K. Searles, A. Zolla, J. Scarborough, and M. Arshadi, *J. Am. Chem. Soc.*, 89, 6393,
868 1967.

869 Kim, T. O., T. Ishida, M. Adachi, K. Okuyama, and J. H. Seinfeld, Nanometer-Sized Particle
870 Formation from $\text{NH}_3/\text{SO}_2/\text{H}_2\text{O}/\text{Air}$ Mixtures by Ionizing Irradiation, *Aerosol Science and*
871 *Technology*, 29, 112-125, 1998.

872 Kirkby, J., Curtius, J., Almeida, J., Dunne, E., Duplissy, J., et al., The role of sulfuric acid,
873 ammonia and galactic cosmic rays in atmospheric aerosol nucleation, *Nature*, 476, 429–433,
874 2011.

875 Korhonen, P., Kulmala, M., Laaksonen, A., Viisanen, Y., McGraw, R., and Seinfeld, J. H., Ternary
876 nucleation of H_2SO_4 , NH_3 , and H_2O in the atmosphere, *J. Geophys. Res.*, 104, 26,349-26,353,
877 1999.

878 Kurtén, T., Torpo, L., Ding, C.-G., Vehkamäki, H., Sundberg, M. R., Laasonen, K., and Kulmala,
879 M.: A density functional study on water-sulfuric acid-ammonia clusters and implications for at-
880 mospheric cluster formation, *J. Geophys. Res.*, 112, D04210, doi:10.1029/2006JD007391,
881 2007.

882 Kürten, A., et al., Experimental particle formation rates spanning tropospheric sulfuric acid and
883 ammonia abundances, ion production rates, and temperatures, *J. Geophys. Res. Atmos.*, 121,
884 12,377–12,400, doi:10.1002/2015JD023908, 2016.

885 Kürten, A., Münch, S., Rondo, L., Bianchi, F., Duplissy, J., Jokinen, T., Junninen, H., Sarnela, N.,
886 Schobesberger, S., Simon, M. and Sipilä, M., Thermodynamics of the formation of sulfuric acid

887 dimers in the binary ($\text{H}_2\text{SO}_4\text{-H}_2\text{O}$) and ternary ($\text{H}_2\text{SO}_4\text{-H}_2\text{O-NH}_3$) system. *Atmospheric*
888 *Chemistry and Physics*, 15(18), pp.10701-10721, 2015.

889 Laakso, L., Mäkelä, J. M., Pirjola, L., and Kulmala, M., Model studies of ion-induced nucleation
890 in the atmosphere, *J. Geophys. Res.*, 107, 4427, doi:10.1029/2002JD002140, 2003.

891 Leverentz, H.R., Siepmann, J.I., Truhlar, D.G., Loukonen, V. and Vehkamäki, H., Energetics of
892 atmospherically implicated clusters made of sulfuric acid, ammonia, and dimethyl amine,
893 *Journal of Physical Chemistry A*, 117(18), 3819-3825, 2013.

894 Lovejoy, E. R., Curtius, J., and Froyd, K. D., Atmospheric ion-induced nucleation of sulfuric acid
895 and water, *J. Geophys. Res.*, 109, D08204, doi:10.1029/2003JD004460, 2004.

896 Ma, Y., Chen, J., Jiang, S., Liu, Y.R., Huang, T., Miao, S.K., Wang, C.Y. and Huang, W.,
897 Characterization of the nucleation precursor ($\text{H}_2\text{SO}_4\text{-(CH}_3)_2\text{NH}$) complex: intra-cluster
898 interactions and atmospheric relevance. *RSC Advances*, 6(7), pp.5824-5836, 2016.

899 Marti, J. J., A. Jefferson, X. Ping Cai, C. Richert, P. H. McMurry, and F. Eisele, H_2SO_4 vapor
900 pressure of sulfuric acid and ammonium sulfate solutions, *J. Geophys. Res.*, 102(D3), 3725–3736,
901 1997.

902 McGrath, M. J., Olenius, T., Ortega, I. K., Loukonen, V., Paasonen, P., Kurtén, T., Kulmala, M.,
903 and Vehkamäki, H.: Atmospheric Cluster Dynamics Code: a flexible method for solution of the
904 birth-death equations, *Atmos. Chem. Phys.*, 12, 2345-2355, doi:10.5194/acp-12-2345-2012,
905 2012.

906 Meng, Z., Xu, X., Lin, W., Xie, Y., Song, B., Jia, S., Zhang, R., Peng, W., Wang, Y., Cheng, H.,
907 Yang, W., and Zhao, H., Role of ambient ammonia in particulate ammonium formation at a rural
908 site in the North China Plain, *Atmos. Chem. Phys. Discuss.*, [https://doi.org/10.5194/acp-2017-](https://doi.org/10.5194/acp-2017-174)
909 174, in review, 2017.

910 Meot-Ner (Mautner), M., The Ionic Hydrogen Bond and Ion Solvation. 2. Hydration of Onium
911 Ions by 1 - 7 H_2O Molecules. Relations Between Monomolecular, Specific and Bulk Hydration,
912 *J. Am. Chem. Soc.*, 106, 5, 1265, 1984.

913 Merikanto J., I. Napari, H. Vehkamäki, T. Anttila, M. Kulmala, New parameterization of sulfuric
914 acid-ammonia-water ternary nucleation rates at tropospheric conditions, *J. Geophys. Res.*, 112,
915 D15207, doi:10.1029/2006JD007977, 2007.

916 Miao, S.K., Jiang, S., Chen, J., Ma, Y., Zhu, Y.P., Wen, Y., Zhang, M.M. and Huang, W.,
917 Hydration of a sulfuric acid–oxalic acid complex: acid dissociation and its atmospheric
918 implication, *RSC Advances*, 5(60), 48638-48646, 2015.

919 Nadykto, A. B., A. Al Natsheh, F. Yu, K.V. Mikkelsen, and J. Herb, Computational Quantum
920 Chemistry: A New Approach to Atmospheric Nucleation, *Advances in Quantum Chemistry*, 55,
921 449-478, 2008.

922 Nadykto, A. B., Al Natsheh, A., Yu, F., Mikkelsen, K. V., and Ruuskanen, J., Quantum nature of
923 the sign preference in the ion-induced nucleation, *Physical Review Letters*, 96, 125701, 2006.

924 Nadykto, A., and Yu, F., Uptake of neutral polar vapour molecules by charged particles:
925 Enhancement due to dipole-charge interaction, *J. Geophys. Res.*, 108(D23), 4717,
926 doi:10.1029/2003JD003664, 2003.

927 Nadykto, A.B. and Yu, F., Strong hydrogen bonding between atmospheric nucleation precursors
928 and common organics. *Chemical physics letters*, 435(1), pp.14-18, 2007a.

929 Nadykto, A.B., Du, H. and Yu, F., Quantum DFT and DF-DFT study of vibrational spectra of
930 sulfuric acid, sulfuric acid monohydrate, formic acid and its cyclic dimer. *Vibrational
931 spectroscopy*, 44(2), pp.286-296, 2007b.

932 Nadykto, A. B., F. Yu, and J. Herb, Theoretical analysis of the gas-phase hydration of common
933 atmospheric pre-nucleation $(\text{HSO}_4^-)(\text{H}_2\text{O})_n$ and $(\text{H}_3\text{O}^+)(\text{H}_2\text{SO}_4)(\text{H}_2\text{O})_n$ cluster ions, *Chemical
934 Physics*, 360, 67-73, doi:10.1016/j.chemphys.2009.04.007, 2009.

935 Nadykto, A.B., Herb, J., Yu, F. and Xu, Y., Enhancement in the production of nucleating clusters
936 due to dimethylamine and large uncertainties in the thermochemistry of amine-enhanced
937 nucleation. *Chemical Physics Letters*, 609, 42-49, 2014.

938 Nadykto, A.B., Herb, J., Yu, F., Nazarenko, E.S. and Xu, Y., Reply to the ‘Comment on
939 “Enhancement in the production of nucleating clusters due to dimethylamine and large
940 uncertainties in the thermochemistry of amine-enhanced nucleation”’ by Kupiainen-Maatta et al.
941 *Chemical Physics Letters*, 624, 111-118, 2015.

942 Napari, I, Noppel, M, Vehkamäki, H., Kulmala, M., An improved model for ternary nucleation of
943 sulfuric acid–ammonia–water. *J. Chem. Phys.*, 116: 4221-4227, DOI: 10.1063/1.1450557, 2002.

944 Olenius T., O. Kupiainen-Määttä, I. K. Ortega, T. Kurtén, and H. Vehkamäki, Free energy barrier
945 in the growth of sulfuric acid–ammonia and sulfuric acid–dimethylamine clusters, *The Journal
946 of Chemical Physics* 2013 139:8, 2013.

947 Ortega, I. K., Kupiainen, O., Kurtén, T., Olenius, T., Wilkman, O., McGrath, M. J., Loukonen, V.,
948 and Vehkamäki, H., From quantum chemical formation free energies to evaporation rates,
949 *Atmos. Chem. Phys.*, 12, 225-235, 2012.

950 Payzant, J.D.; Cunningham, A.J.; Kebarle, P., Gas - Phase Solvation of Ammonium Ion by NH_3
951 and H_2O and Stabilities of Mixed Clusters $\text{NH}_4^+(\text{NH}_3)_n(\text{H}_2\text{O})_w$, *Can. J. Chem.*, 51, 19, 3242,
952 1973.

953 Peng, X.Q., Liu, Y.R., Huang, T., Jiang, S. and Huang, W., Interaction of gas phase oxalic acid
954 with ammonia and its atmospheric implications, *Physical Chemistry Chemical Physics*, 17(14),
955 9552-9563, 2015.

956 Raes, F., A. Janssens, and R. V. Dingenen, The role of ion-induced aerosol formation in the lower
957 atmosphere, *J. Aerosol Sci.*, 17, 466–470, 1986.

958 Schnitzhofer, R., et al., Characterisation of organic contaminants in the CLOUD chamber at
959 CERN, *Atmos. Meas. Tech.*, 7, 2159–2168, doi:10.5194/amt-7-2159-2014, 2014.

960 Schobesberger, S., et al., On the composition of ammonia–sulfuric-acid ion clusters during aerosol
961 particle formation, *Atmos. Chem. Phys.*, 15, 55-78, <https://doi.org/10.5194/acp-15-55-2015>,
962 2015.

963 Sipilä, M., Berndt, T., Petäjä, T., Brus, D., Vanhanen, J., Stratmann, F., Patokoski, J.,
964 Mauldin, R. L., Hyvärinen, A. P., Lihavainen, H., and Kulmala, M.: The Role of
965 Sulfuric Acid in Atmospheric Nucleation, *Science*, 327, 1243,
966 <https://doi.org/10.1126/science.1180315>, 2010.

967 Sorokin, A., Arnold, F. and Wiedner, D., Formation and growth of sulfuric acid–water cluster ions:
968 Experiments, modelling, and implications for ion-induced aerosol formation, *Atmospheric*
969 *Environment*, 40, 2030-2045, 2006.

970 Temelso, B., Morrell, T.E., Shields, R.M., Allodi, M.A., Wood, E.K., Kirschner, K.N.,
971 Castonguay, T.C., Archer, K.A. and Shields, G.C., Quantum mechanical study of sulfuric acid
972 hydration: Atmospheric implications. *The Journal of Physical Chemistry A*, 116(9), 2209-2224,
973 2012a.

974 Temelso, B., Phan, T.N. and Shields, G.C., Computational study of the hydration of sulfuric acid
975 dimers: Implications for acid dissociation and aerosol formation, *Journal of Physical Chemistry*
976 *A*, 116(39), pp.9745-9758, 2012b.

977 Thomson, J. J., *Applications of Dynamics to Physics and Chemistry*, 1st ed., Cambridge University
978 Press, London, 1888.

979 Torpo, L., Kurtén, T., Vehkamäki, H., Laasonen, K., Sundberg, M.R. and Kulmala, M.,
980 Significance of ammonia in growth of atmospheric nanoclusters. *The Journal of Physical*
981 *Chemistry A*, 111(42), pp.10671-10674, 2007.

982 Vehkamäki H., Kulmala, M., Napari, I., Lehtinen, K. E. J., Timmreck, C., Noppel, M., and
983 Laaksonen, A., An improved parameterization for sulfuric acid–water nucleation rates for
984 tropospheric and stratospheric conditions, *J. Geophys. Res.*, 107 (D22), 4622,
985 doi:10.1029/2002JD002184, 2002.

986 Warner, J. X., Wei, Z., Strow, L. L., Dickerson, R. R., & Nowak, J. B.. The global tropospheric
987 ammonia distribution as seen in the 13-year AIRS measurement record. *Atmospheric Chemistry*
988 *and Physics*, 16(8), 5467-5479. <https://doi.org/10.5194/acp-16-5467-2016>, 2016.

989 Wilhelm, S., Eichkorn, S., Wiedner, D., Pirjola, L. and Arnold, F.: Ion-induced aerosol formation:
990 new insights from laboratory measurements of mixed cluster ions, $\text{HSO}_4^-(\text{H}_2\text{SO}_4)_a(\text{H}_2\text{O})_w$ and
991 $\text{H}^+(\text{H}_2\text{SO}_4)_a(\text{H}_2\text{O})_w$, *Atmos. Environ.*, 38, 1735-1744, 2004.

992 Włodek, S., Z. Łuczyński, H. Wincel, Stabilities of gas-phase NO_3^- (HNO_3)_n, $n \leq 6$, clusters, In
993 International Journal of Mass Spectrometry and Ion Physics, 35, 1–2, 1980, 39-46, 1980.

994 Xu, W. and Zhang, R., A theoretical study of hydrated molecular clusters of amines and
995 dicarboxylic acids, Journal of chemical physics, 139(6), p.064312, 2013.

996 Xu, W. and Zhang, R., Theoretical investigation of interaction of dicarboxylic acids with common
997 aerosol nucleation precursors, Journal of Physical Chemistry A, 116(18), 4539-4550, 2012.

998 Yu, F., and Turco, R. P., The role of ions in the formation and evolution of particles in aircraft
999 plumes, Geophys. Res. Lett., 24, 1927-1930, 1997.

1000 Yu, F., and Turco, R. P., Ultrafine aerosol formation via ion-mediated nucleation, Geophys. Res.
1001 Lett., 27, 883-886, 2000.

1002 Yu, F., and R. P. Turco: From molecular clusters to nanoparticles: The role of ambient ionization
1003 in tropospheric aerosol formation, J. Geophys. Res., 106, 4797-4814, 2001.

1004 Yu, F. and Turco, R. P., The size-dependent charge fraction of sub-3-nm particles as a key
1005 diagnostic of competitive nucleation mechanisms under atmospheric conditions, Atmos. Chem.
1006 Phys., 11, 9451–9463, doi:10.5194/acp-11-9451-2011, 2011.

1007 Yu, F., Modified Kelvin-Thomson equation considering ion-dipole interaction: Comparison with
1008 observed ion-clustering enthalpies and entropies, J. Chem. Phys., 122, 084503, 2005.

1009 Yu, F., Effect of ammonia on new particle formation: A kinetic H_2SO_4 - H_2O - NH_3 nucleation model
1010 constrained by laboratory measurements, J. Geophys. Res., 111, D01204,
1011 doi:10.1029/2005JD005968, 2006a.

1012 Yu, F., From molecular clusters to nanoparticles: Second-generation ion-mediated nucleation
1013 model, Atmos. Chem. Phys., 6, 5193-5211, 2006b.

1014 Yu, F., Improved quasi-unary nucleation model for binary H_2SO_4 - H_2O homogeneous nucleation,
1015 J. Chem. Phys., 127, 054301, 2007.

1016 Zhang, R, Khalizov, AF, Wang, L, Hu, M, Wen, X., Nucleation and growth of nanoparticles in the
1017 atmosphere, Chem. Rev. 112: 1957-2011, DOI: 10.1021/cr2001756, 2012.

1018 Zhang, R., Wang, L., Khalizov, A.F., Zhao, J., Zheng, J., McGraw, R.L. and Molina, L.T.,
1019 Formation of nanoparticles of blue haze enhanced by anthropogenic pollution, Proceedings of
1020 the National Academy of Sciences, 106(42), 17650-17654, 2009.

1021 Zhang, Y., P. H. McMurry, F. Yu, and M. Z. Jacobson, A Comparative Study of Homogeneous
1022 Nucleation Parameterizations, Part I. Examination and Evaluation of the Formulations, J.
1023 Geophys. Res., 115, D20212, doi:10.1029/2010JD014150, 2010.

1024 Zhu, Y.P., Liu, Y.R., Huang, T., Jiang, S., Xu, K.M., Wen, H., Zhang, W.J. and Huang, W.,
1025 Theoretical study of the hydration of atmospheric nucleation precursors with acetic acid, Journal
1026 of Physical Chemistry A, 118(36), 7959-7974, 2014.

1027 Zollner, J. H., W. A. Glasoe, B. Panta, K. K. Carlson, P. H. McMurry, and D. R. Hanson, Sulfuric
1028 acid nucleation: Power dependencies, variation with relative humidity, and effect of bases,
1029 Atmos. Chem. Phys., 12(10), 4399–4411, doi:10.5194/acp-12-4399-2012, 2012.
1030

1031 **Table A1.** Number of isomers successfully converged at 6-311 level for selected clusters, along
 1032 with the enthalpy, entropy, and Gibbs free energy of the most stable isomers.
 1033

Cluster Formula	6-311++ conv.	Enthalpy (Hartree)	Entropy (cal/K·mol)	Gibbs free energy (Hartree)
S ₄	56	-2801.256008	179.461	-2801.341276
S ₄ A ₁	169	-2857.820795	187.395	-2857.909833
S ₄ A ₂	84	-2914.388489	193.997	-2914.480663
S ₄ A ₃	68	-2970.94645	209.77	-2971.046119
S ₄ A ₄	38	-3027.500303	225.959	-3027.607663
S ₄ A ₅	34	-3084.050337	237.758	-3084.163303
S ⁻ S ₃	97	-2800.835072	168.993	-2800.915366
S ⁻ S ₃ A ₁	122	-2857.389946	184.899	-2857.477797
S ⁻ S ₃ A ₂	21	-2913.941409	192.489	-2914.032867
S ⁻ S ₃ A ₃	13	-2970.490814	195.627	-2970.583762
S ⁻ S ₄	138	-3501.162655	200.525	-3501.257931
S ⁻ S ₄ A ₁	71	-3557.727072	208.015	-3557.825907
S ⁻ S ₄ A ₂	22	-3614.287482	213.397	-3614.388874
S ⁻ S ₄ A ₃	23	-3670.836831	226.504	-3670.94445
S ⁻ S ₄ A ₄	18	-3727.385956	237.152	-3727.498634
H ⁺ A ₂	16	-113.413269	68.478	-113.445805
H ⁺ A ₂ W ₁	42	-189.845603	94.248	-189.890384
H ⁺ A ₂ W ₂	56	-266.276653	113.49	-266.330576
H ⁺ A ₂ W ₃	63	-342.706301	132.722	-342.769362
H ⁺ A ₂ W ₄	114	-419.133157	160.449	-419.209391
H ⁺ A ₂ W ₅	116	-495.567408	161.447	-495.644117
H ⁺ A ₂ W ₆	70	-571.994961	175.085	-572.078149
H ⁺ A ₂ W ₀ S ₁	40	-813.745253	107.764	-813.796455
H ⁺ A ₂ W ₁ S ₁	173	-890.181285	121.33	-890.238933
H ⁺ A ₂ W ₂ S ₁	103	-966.618165	130.584	-966.680209
H ⁺ A ₂ W ₃ S ₁	169	-1043.047622	154.145	-1043.120861
H ⁺ A ₂ W ₄ S ₁	188	-1119.476882	177.051	-1119.561004
H ⁺ A ₂ W ₅ S ₁	178	-1195.90253	200.029	-1195.99757
H ⁺ A ₂ W ₆ S ₁	85	-1272.330781	215.117	-1272.43299

1034

1035 **Table A2.** QC-based stepwise Gibbs free energy change (in kcal/mol) for the addition of one
 1036 water (ΔG_{+W}°), ammonia (ΔG_{+A}°), or sulfuric acid (ΔG_{+S}°) molecule to form the given positively
 1037 charged clusters under standard conditions, and the corresponding experimental data or semi-
 1038 experimental estimates.
 1039

	ΔG_{+W}°		ΔG_{+A}°		ΔG_{+S}°	
	QC	experimental	QC	experimental	QC	experimental
$H^+W_1S_1$					-28.59	-24.65 ^f
$H^+W_2S_1$	-15.66				-15.33	-13.76 ^f
$H^+W_3S_1$	-9.40				-10.12	-11.93 ^f
$H^+W_4S_1$	-7.83				-9.18	-9.71 ^f
$H^+W_5S_1$	-6.77	-5.79 ^a			-9.52	-9.82 ^f
$H^+W_6S_1$	-5.32	-4.24 ^a			-9.70	-9.94 ^f
$H^+W_7S_1$	-3.18	-3.28 ^a			-9.64	-9.96 ^f
$H^+W_8S_1$	-2.80	-2.67 ^a			-9.84	-10.10 ^f
$H^+W_9S_1$	-2.30	-2.12 ^a			-10.24	-10.86 ^f
$H^+A_1W_1$	-13.47	-13.01 ^b , -11.43 ^c	-52.08			
$H^+A_1W_2$	-9.85	-7.14 ^b , -8.17 ^c	-33.02			
$H^+A_1W_3$	-6.60	-5.92 ^b , -5.88 ^c	-25.01			
$H^+A_1W_4$	-3.50	-3.94 ^b , -4.06 ^c	-19.73			
$H^+A_1W_5$	-2.50	-2.55 ^b , -3.02 ^c	-15.80			
$H^+A_1W_6$	-2.26	-2.54 ^b	-12.93			
$H^+A_1W_7$	-1.15	-1.84 ^b	-10.84			
$H^+A_1W_8$	-1.02		-9.26			
$H^+A_1W_9$	0.25		-8.32			
H^+A_2			-22.97	-18.25 ^c		
$H^+A_2W_1$	-7.04	-6.85 ^c	-16.53	-11.54 ^c , -12.75 ^d		
$H^+A_2W_2$	-4.29	-5.25 ^c	-10.97	-9.13 ^c , -9.50 ^d		
$H^+A_2W_3$	-3.41	-3.70 ^c	-7.78	-6.83 ^c , -7.02 ^d		
$H^+A_2W_4$	-3.08		-7.36			
$H^+A_2W_5$	-1.97		-6.82			
$H^+A_2W_6$	-0.42		-4.99			
$H^+A_1W_1S_1$	-8.99		-33.14		-9.65	-8.3 ^d
$H^+A_1W_2S_1$	-8.11		-25.59		-7.90	-7.1 ^d
$H^+A_1W_3S_1$	-6.09		-22.28		-7.40	-6.7 ^d
$H^+A_1W_4S_1$	-4.25		-18.71		-8.15	-6.9 ^d
$H^+A_1W_5S_1$	-1.92		-13.85		-7.56	-7.5 ^d
$H^+A_1W_6S_1$	-2.04		-10.57		-7.34	-8.0 ^d
$H^+A_2W_0S_1$			-22.09	-22.14 ^e	-13.35	-16.8 ^d

H ⁺ A ₂ W ₁ S ₁	-5.72	-18.92	-12.03	-15.8 ^d
H ⁺ A ₂ W ₂ S ₁	-4.97	-15.78	-12.71	-15.9 ^d
H ⁺ A ₂ W ₃ S ₁	-4.58	-14.27	-13.89	-16.3 ^d
H ⁺ A ₂ W ₄ S ₁	-4.26	-14.27	-15.06	-17.3 ^d
H ⁺ A ₂ W ₅ S ₁	-2.01	-14.37	-15.11	-18.8 ^d
H ⁺ A ₂ W ₆ S ₁	-1.29	-13.63	-15.98	-19.9 ^d

1040 ^a Froyd and Lovejoy, 2003; ^b Meot-Ner (Mautner) et al., 1984; ^c Payzant et al., 1973; ^d Froyd, 2002; ^e

1041 Froyd and Lovejoy, 2012. ^f The ΔG_{+S}° values given here were calculated based on experimental ΔG_{+S}°

1042 values at T=270 K from Froyd and Lovejoy (2003) and ΔS values from quantum calculation.

1043

1044 **Table A3.** Same as Table A2 except for neutral clusters.

1045

	ΔG_{+W}°		ΔG_{+A}°		ΔG_{+S}°	
	QC	experimental	QC	experimental	QC	experimental
S ₁ A ₁			-7.77 ^a (-7.29 ^b , -7.61 ^c , -6.60 ^d)	-8.2 ^e	-7.77 ^a (-7.29 ^b , -7.61 ^c , -6.60 ^d)	-8.2 ^e
S ₁ A ₁ W ₁	-1.39 ^a		-6.88 ^a			
S ₁ A ₁ W ₂	-2.30 ^a		-6.18 ^a			
S ₁ A ₁ W ₃	-1.52 ^a		-5.81 ^a			
S ₁ A ₂			-4.75			
S ₁ A ₂ W ₁	-0.78		-4.15			
S ₂ A ₁			-13.84 ^a		-11.65 ^a	
S ₂ A ₁ W ₁	-2.31 ^a		-12.77		-12.59 ^a	
S ₂ A ₁ W ₂	-1.21 ^a		-11.00		-11.52 ^a	
S ₂ A ₁ W ₃	-2.04 ^a		-9.69		-12.04 ^a	
S ₂ A ₂			-8.75		-15.65	
S ₂ A ₂ W ₁	-1.96		-8.37		-16.83	
S ₂ A ₂ W ₂	-1.19		-8.35		-15.49	
S ₂ A ₂ W ₃	0.60		-5.71		-14.42	
S ₂ A ₃			-4.19			
S ₃ A ₁			-16.14		-7.08	
S ₃ A ₂			-13.84		-12.17	
S ₃ A ₃			-8.93		-16.92	
S ₃ A ₄			-7.42			
S ₄ A ₁			-15.74		-4.16	
S ₄ A ₂			-17.16		-7.48	
S ₄ A ₃			-13.79		-12.34	
S ₄ A ₄			-11.34		-16.26	
S ₄ A ₅			-7.63			

1046 ^a Nadykto and Yu, 2007; ^b Torpo et al., 2007; ^c Ortega et al., 2012; ^d Chon et al., 2007; ^e Kurten et al.,
 1047 2015.

1048

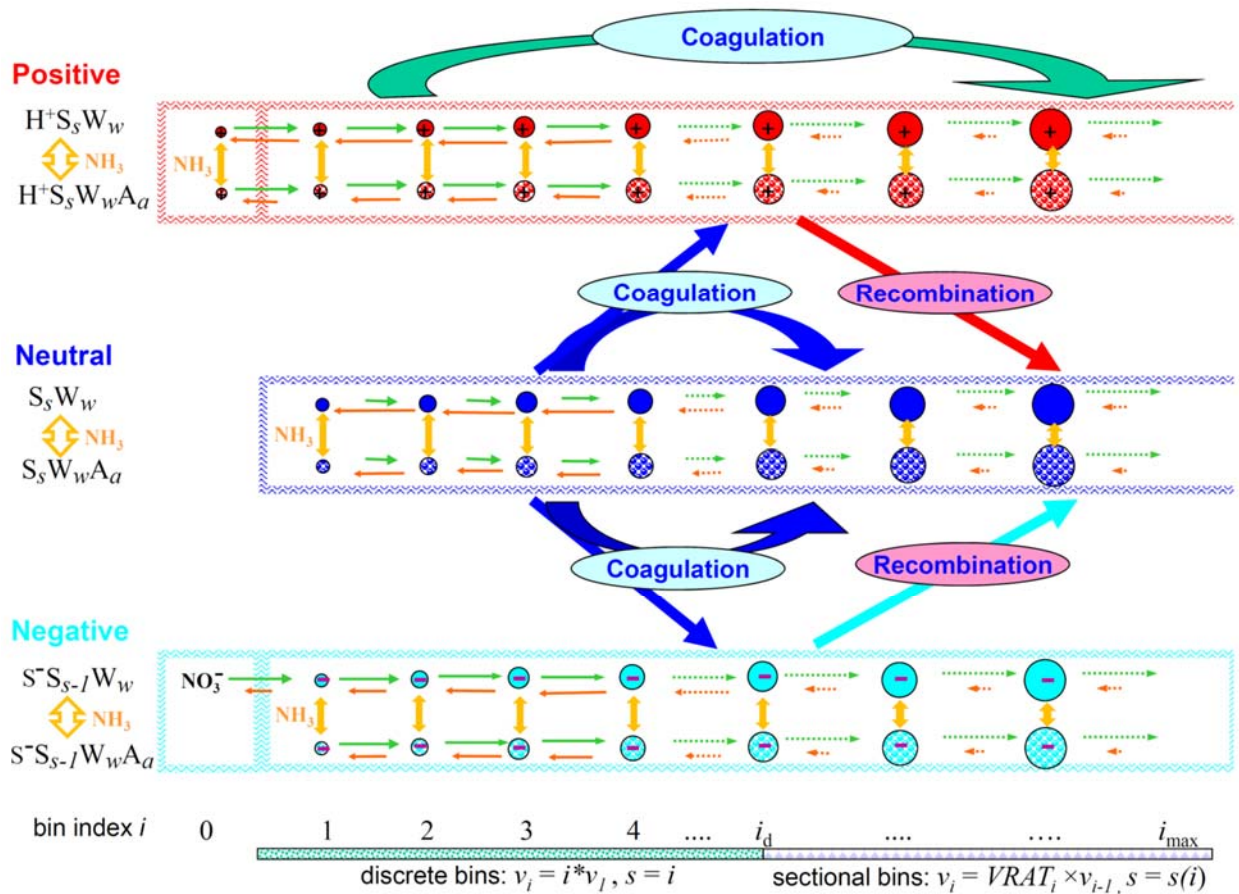
1049 **Table A4.** Same as Table A2 except for negatively charged clusters.

1050

	ΔG_{+W}°		$\Delta G_{+\Delta}^{\circ}$		ΔG_{+S}°	
	QC	experimental	QC	experimental	QC	experimental
S ⁻ A ₁			2.81			
S ⁻ S ₁ W ₀					-32.74	-29.10 ^a
S ⁻ S ₁ W ₁	-0.61				-28.12	
S ⁻ S ₁ W ₂	-1.06				-25.36	
S ⁻ S ₁ A ₁			0.08		-35.47	
S ⁻ S ₂ W ₀					-15.06	-17.14 ^a
S ⁻ S ₂ W ₁	-1.83				-16.28	
S ⁻ S ₂ A ₁			-4.85		-19.99	
S ⁻ S ₃ W ₀					-10.58	-13.28 ^a
S ⁻ S ₃ W ₁	-2.92	-2.73 ^a			-11.67	-14.29 ^a
S ⁻ S ₃ W ₂	-2.03	-1.53 ^a			-11.12	-13.80 ^a
S ⁻ S ₃ W ₃	-2.01	-1.93 ^a			-11.52	-14.72 ^a
S ⁻ S ₃ W ₄	-1.73					
S ⁻ S ₃ A ₁ W ₀			-11.89		-17.62	
S ⁻ S ₃ A ₁ W ₁	0.52		-8.45		-14.90	
S ⁻ S ₃ A ₁ W ₂	0.39		-6.03		-13.06	
S ⁻ S ₃ A ₂			-7.27		-18.36	
S ⁻ S ₃ A ₃			-4.66			
S ⁻ S ₄ W ₀					-8.28	-10.96 ^a
S ⁻ S ₄ W ₁	-3.50	-2.61 ^a			-8.86	-10.71 ^a
S ⁻ S ₄ W ₂	-3.17	-2.79 ^a			-9.99	-12.10 ^a
S ⁻ S ₄ W ₃	-2.65	-2.41 ^a			-10.64	-12.48 ^a
S ⁻ S ₄ W ₄	-2.25	-2.14 ^a			-11.16	-12.77 ^a
S ⁻ S ₄ A ₁ W ₀			-15.37		-11.76	
S ⁻ S ₄ A ₁ W ₁	-2.21		-14.09		-14.49	
S ⁻ S ₄ A ₁ W ₂	-0.74		-11.66		-15.62	
S ⁻ S ₄ A ₂			-12.23		-16.71	
S ⁻ S ₄ A ₃			-7.59		-19.65	
S ⁻ S ₄ A ₄			-6.72			

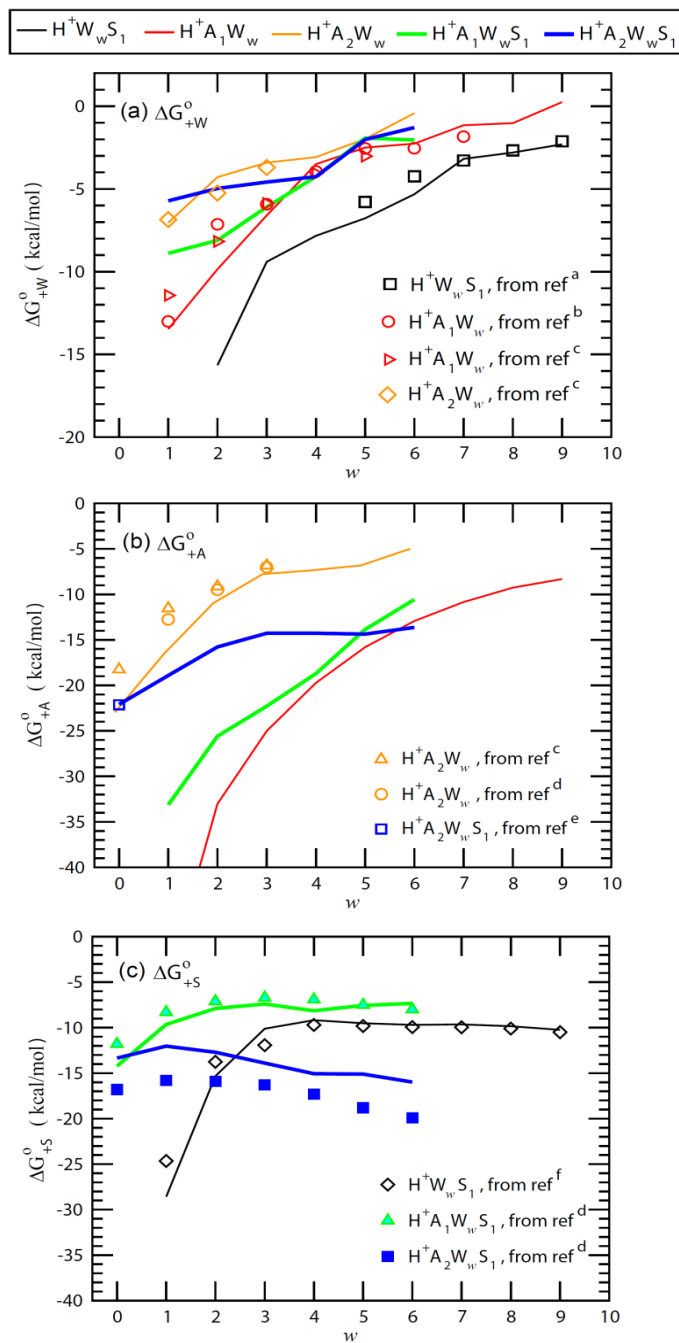
1051 ^a Froyd and Lovejoy, 2003.

1052



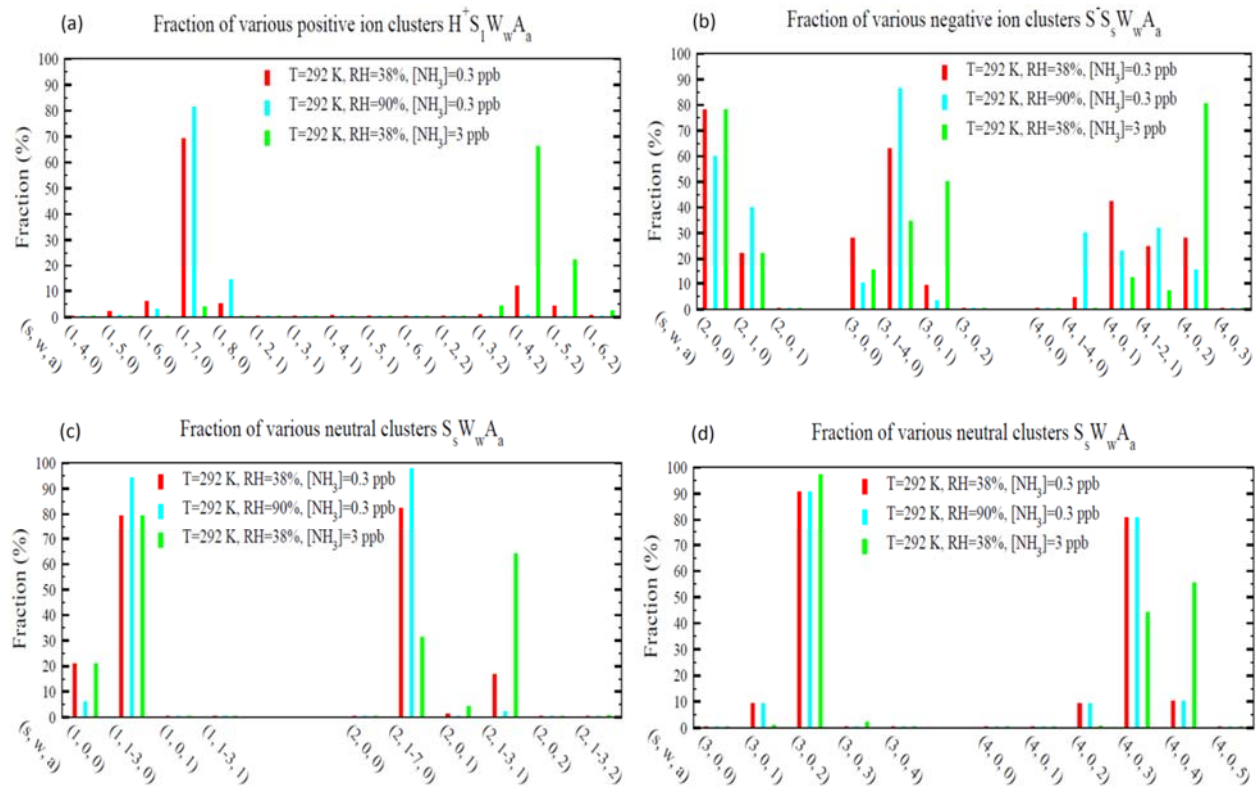
1053
1054

1055 **Figure 1.** Schematic illustration of kinetic processes controlling the evolution of positively
 1056 charged ($H^+S_sW_wA_a$), neutral ($S_sW_wA_a$), and negatively charged ($S^-S_{s-1}W_wA_a$)
 1057 clusters/droplets that are explicitly simulated in the ternary ion-mediated nucleation (TIMN)
 1058 model. Here S, W, and A represent sulfuric acid (H_2SO_4), water (H_2O), and ammonia (NH_3)
 1059 respectively, while s , w , and a refer to the number of S, W, and A molecules in the clusters/droplets,
 1060 respectively. The TIMN model has been extended from an earlier version treating binary IMN
 1061 (BIMN) by adding NH_3 into the nucleation system and using a discrete-sectional bin structure to
 1062 represent the sizes of clusters/particles starting from a single molecule up to background particles
 1063 larger than a few micrometers.



1064
1065 **Figure 2.** Stepwise Gibbs free energy change under standard conditions for the addition of a water
1066 (ΔG°_{+W}), ammonia (ΔG°_{+A}), or sulfuric acid (ΔG°_{+S}) molecule to form the given positively charged
1067 clusters as a function of the number of water molecules in the clusters (w). Lines are QC-based
1068 values, and symbols are experimental results or semi-experimental estimates (see notes under
1069 Table A2 for the references).

1070



1071

1072

Figure 3. Relative abundance (or molar fraction) of small clusters containing a given number of

1073

H₂SO₄ molecules for positive, negative, and neutral cluster types at a temperature of 292 K and

1074

three different combinations of RHs (38% and 90%) and [NH₃] (0.3 and 3 ppb). Some clusters

1075

with different numbers of water molecules were grouped together to make the plot more clear and

1076

neat. For the clusters shown in panel (d), there is no hydrate data and thus hydration for these

1077

clusters were not calculated.

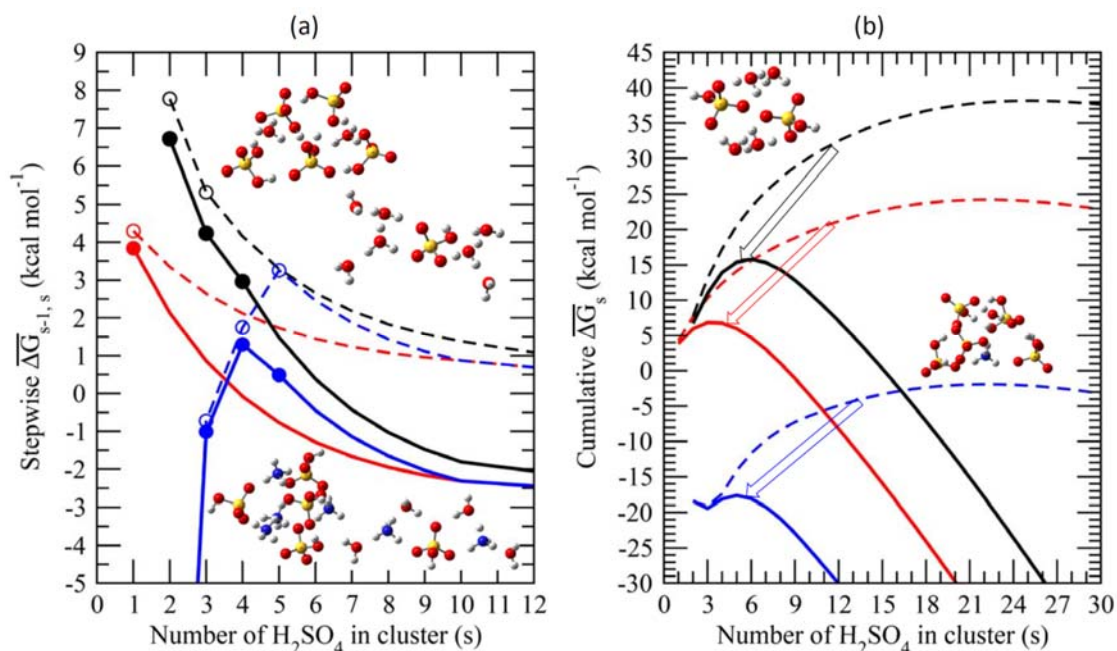
1078

1079

1080

1081

1082



1083

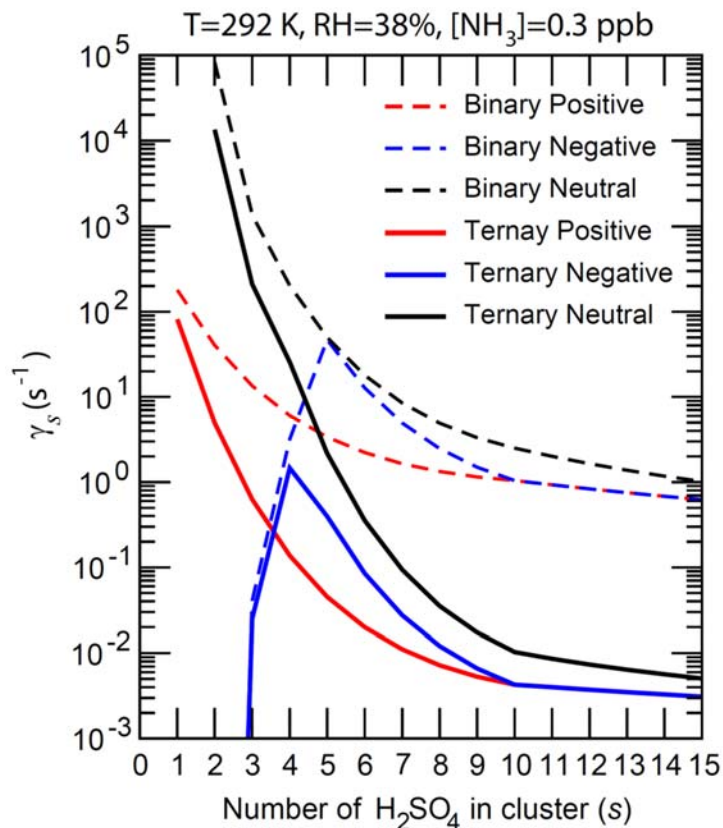
1084 **Figure 4.** (a) Average stepwise Gibbs free energy change for the addition of one H₂SO₄ molecule1085 to form a neutral (black), positively charged (red), or negatively charged (blue) binary H₂SO₄-H₂O1086 (dashed lines or empty circles) or ternary H₂SO₄-H₂O-NH₃ (solid lines or filled circles) cluster1087 containing s H₂SO₄ molecules ($\overline{\Delta G}_{s-1,s}$); (b) Same as (a) but for the cumulative (total) Gibbs free1088 energy change in each case. Filled and empty circles in (a) refer to $\overline{\Delta G}_{s-1,s}$ obtained using1089 measurements and/or quantum-chemical calculations. $\overline{\Delta G}_{s-1,s}$ for larger clusters with $s \geq 10$, which

1090 approach the properties of the equivalent bulk liquid (20), are calculated using the capillarity

1091 approximation. Interpolation is used to calculate $\overline{\Delta G}_{s-1,s}$ for clusters up to $s=10$ (Eq. 11).1092 Calculations were carried out at T=292 K, RH=38%, [H₂SO₄]=3×10⁸ cm⁻³ and [NH₃]= 0.3 ppb.

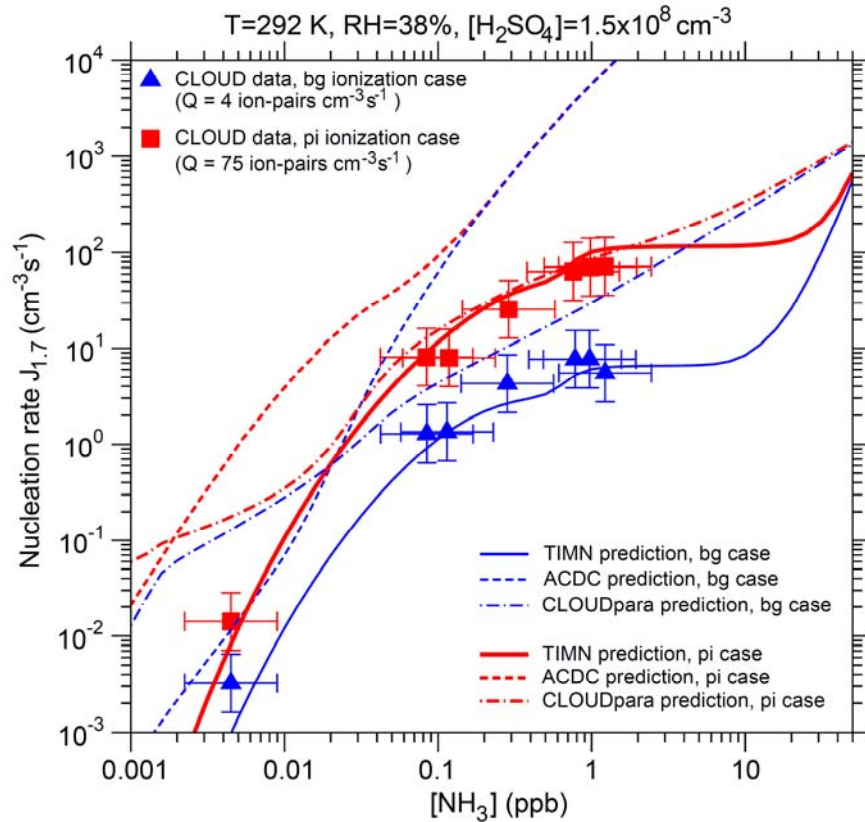
1093 The inset diagrams represent equilibrium geometries for the most stable isomers of selected binary

1094 clusters ($(\text{H}_3\text{O}^+)(\text{H}_2\text{SO}_4)(\text{H}_2\text{O})_6$, $(\text{H}_2\text{SO}_4)_2(\text{H}_2\text{O})_4$, and $(\text{HSO}_4^-)(\text{H}_2\text{SO}_4)_4(\text{H}_2\text{O})_2$), and ternary
 1095 clusters ($(\text{NH}_4^+)(\text{H}_2\text{SO}_4)(\text{NH}_3)(\text{H}_2\text{O})_4$, $(\text{HSO}_4^-)(\text{H}_2\text{SO}_4)_4(\text{H}_2\text{O})(\text{NH}_3)$, $(\text{H}_2\text{SO}_4)_4(\text{NH}_3)_4$).



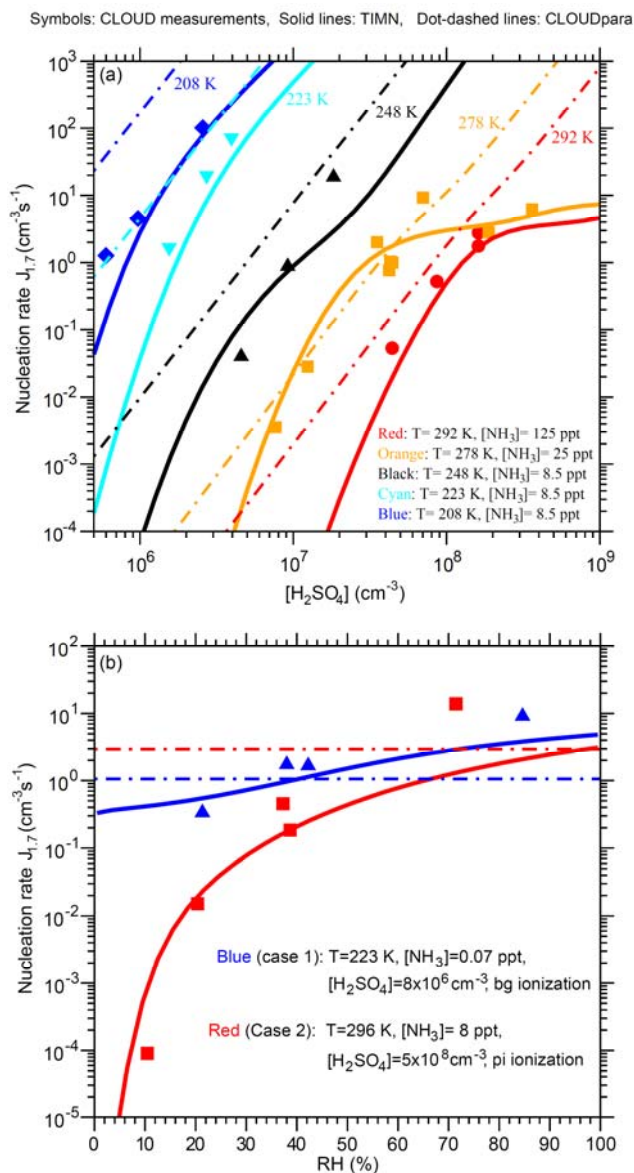
1096
 1097 **Figure 5.** The number-concentration-weighted mean evaporation rates ($\bar{\gamma}$) of H_2SO_4 molecules
 1098 from neutral clusters (black), positively charged clusters (red), and negatively charged clusters
 1099 (blue) for binary (H_2SO_4 - H_2O , dashed lines) and ternary (H_2SO_4 - H_2O - NH_3 , solid lines) nucleating
 1100 systems containing s H_2SO_4 molecules ($\overline{\Delta G_{s-1,s}}$). $T=292$ K, $\text{RH}=38\%$, and $[\text{NH}_3] = 0.3$ ppb for
 1101 the ternary system.

1102
 1103
 1104



1105

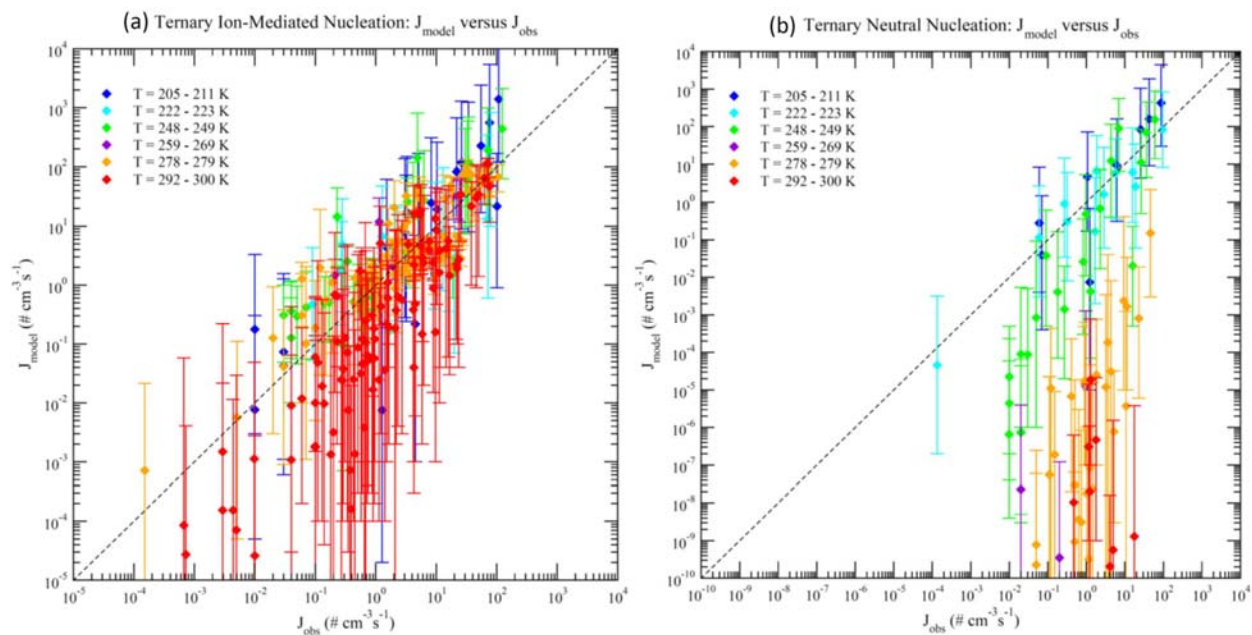
1106 **Figure 6.** Effect of ammonia concentrations ($[\text{NH}_3]$) on effective nucleation rates calculated at a
 1107 cluster mobility diameter of 1.7 nm ($J_{1.7}$, lines) under the stated conditions with two ionization
 1108 rates (Q) – background ionization, bg (blue), and ionization enhanced by a pion beam, pi (red).
 1109 Also shown are predictions from the TIMN model, the Atmospheric Cluster Dynamics Code
 1110 (ACDC) with thermochemistry obtained using RI-CC2//B3LYP method (McGrath et al., 2012;
 1111 Kurten et al., 2016), and an empirical parameterization of CLOUD measurements (CLOUDpara)
 1112 (Dunne et al., 2016) are indicated by solid, dashed, and dot-dashed lines, respectively. The symbols
 1113 refer to CLOUD experimental data (Kirkby et al., 2011; Dunne et al., 2016), with the uncertainties
 1114 in measured $[\text{NH}_3]$ and $J_{1.7}$ shown by horizontal and vertical bars, respectively. To be comparable,
 1115 the CLOUD data points given in Dunne et al. (2016) under the conditions of $T=292$ K and
 1116 $\text{RH}=38\%$ with $[\text{H}_2\text{SO}_4]$ close to $1.5 \times 10^8 \text{ cm}^{-3}$ have been interpolated to the same $[\text{H}_2\text{SO}_4]$ value
 1117 ($=1.5 \times 10^8 \text{ cm}^{-3}$).



1118

1119 **Figure 7.** Comparison of TIMN simulations (solid lines), CLOUDpara predictions (Dunne et al.,
 1120 2016) (dot-dashed lines) and CLOUD measurements (symbols, data from Dunne et al. (2016) of
 1121 the dependences of nucleation rates on (a) $[\text{H}_2\text{SO}_4]$ at five different temperatures ($T = 292, 278,$
 1122 $248, 223,$ and 208 K) and (b) RH at two sets of conditions as specified. $[\text{NH}_3]$ is in ppt (parts per
 1123 trillion, by volume). Error bars for the uncertainties in measured $[\text{H}_2\text{SO}_4]$ (-50%, +100%), $[\text{NH}_3]$
 1124 (-50%, +100%), and $J_{1.7}$ (overall a factor of two) are not shown. To be comparable, the CLOUD
 1125 data points given in Dunne et al. (2016) under the conditions ($T, \text{RH},$ ionization rate) with $[\text{NH}_3]$
 1126 or $[\text{H}_2\text{SO}_4]$ close to the corresponding values specified in the figure legends have been interpolated
 1127 to the same $[\text{NH}_3]$ (Fig. 7a) or $[\text{H}_2\text{SO}_4]$ (Fig. 7b) values.

1128



1130

1131 **Figure 8.** Model predicted (J_{model}) versus observed (J_{obs}) nucleation rates under various conditions
 1132 of all 377 data points of CLOUD measurements reported in Table S1 of Dunne et al. (2016), with
 1133 (a) and without (b) the presence of ionization. The data points are grouped according to
 1134 temperatures as specified in the legend. Vertical error bars show the range of J_{model} calculated at
 1135 50% and 200% of measured $[\text{H}_2\text{SO}_4]$, corresponding to the uncertainties in measured $[\text{H}_2\text{SO}_4]$ (-
 1136 50%, +100%). Error bars associated with the uncertainties in measured $[\text{NH}_3]$ (-50%, +100%), and
 1137 J_{obs} (overall a factor of two) are not shown.